Randomly evolving idiotypic networks: Structural properties and architecture

Holger Schmidtchen,[1,2] Mario Thüne,[1] and Ulrich Behn[1,2,*]

[1]*Institut für Theoretische Physik, Universität Leipzig, POB 100 920, D-04009 Leipzig, Germany*

[2]*International Max Planck Research School Mathematics in the Sciences, Inselstraße 22, D-04103 Leipzig, Germany*

(Received 16 January 2012; published 31 July 2012)

We consider a minimalistic dynamic model of the idiotypic network of B lymphocytes. A network node represents a population of B lymphocytes of the same specificity (idiotype), which is encoded by a bit string. The links of the network connect nodes with complementary and nearly complementary bit strings, allowing for a few mismatches. A node is occupied if a lymphocyte clone of the corresponding idiotype exists; otherwise it is empty. There is a continuous influx of new B lymphocytes of random idiotype from the bone marrow. B lymphocytes are stimulated by cross-linking their receptors with complementary structures. If there are too many complementary structures, steric hindrance prevents cross-linking. Stimulated cells proliferate and secrete antibodies of the same idiotype as their receptors; unstimulated lymphocytes die. Depending on few parameters, the autonomous system evolves randomly towards patterns of highly organized architecture, where the nodes can be classified into groups according to their statistical properties. We observe and describe analytically the building principles of these patterns, which make it possible to calculate number and size of the node groups and the number of links between them. The architecture of all patterns observed so far in simulations can be explained this way. A tool for real-time pattern identification is proposed.

DOI: 10.1103/PhysRevE.86.011930 PACS number(s): 87.18.−h, 87.23.Kg, 64.60.aq, 02.70.Rr

I. INTRODUCTION

B lymphocytes play a crucial role in the adaptive immune system. They express Y-shaped receptor molecules, antibodies, on their surface. Antibodies have very specific binding sites (*idiotopes*) which determine their *idiotype*. All receptors of a given B cell have the same idiotype. B cells are stimulated to proliferate if their receptors are cross-linked by structures which are complementary to the idiotopes, for example, by foreign antigen. Stimulated B cells thus survive, whereas unstimulated B cells die; this process is called clonal selection [1].

After a few generations, stimulated B cells differentiate to plasma cells which secrete soluble antibody molecules of the same idiotype, which may bind to complementary sites on antigen and mark them for further processing.

B lymphocytes of different idiotype are continuously produced in the bone marrow in a remarkable diversity. The variety of the potential idiotype repertoire, created by somatic reshuffling of gene segments and mutations [2], was combinatorially estimated [3] to exceed most likely 10^{10}.

Complementary structures may be found on antigen but could also be situated on other antibodies of complementary idiotype. B lymphocytes can stimulate each other and, thus, as conceived by Jerne [4], they form a functional network, the *idiotypic network*.

The concept of the idiotypic network explains in a natural way the diversity of the expressed idiotype repertoire and the autonomous dynamics of an immune system not exposed to foreign antigen. It provides a mechanism of immunological memory. Imagine that an antigen Ag is recognized by an antibody Ab_1. Thus, the clone of Ab_1 expands and possibly meets another clone of complementary idiotype Ab_2. Both mutually stimulate each other and they persist even after Ag has disappeared. Ab_2 is structurally similar to Ag and can be considered as internal image of Ag. Furthermore, the network is thought to control autoreactive clones. All these issues are beyond the concept of clonal selection.

The network paradigm got an immediate enthusiastic response and idiotypic interactions were considered as the major regulating mechanism of the immune system. However, the rapid progress of molecular immunology, difficulties in the direct experimental verification, and the discovery of other regulating mechanisms let the interest of experimental immunologists decay. Yet, for system biologists the network paradigm always remained attractive. Several aspects of the original concept were revised in due course. Most notably, Varela and Coutinho [5–7] suggested second-generation networks with an architecture comprising a strongly connected central part with autonomous dynamics and a sparsely connected peripheral part for localized memory and adaptive immune response. In a sense, they reconcile both paradigms of idiotypic networks and clonal selection. A readable history of immunological paradigms can be found in [8]. Reviews with focus on idiotypic networks are [9] with an emphasis on modeling approaches and more recently [10] with emphasis on new immunological and clinical developments.

Today, the main activities are in clinical research. Idiotypic interactions are the base of all therapies with monoclonal antibodies [11]. New experimental techniques make large-scale studies of the idiotypic repertoire feasible [12], which are necessary to infer the networks architecture.

In this paper we consider a minimalistic model of the idiotypic network, which was first formulated and investigated in [13]. In this model a node represents lymphocytes and antibodies of a given idiotype. Lymphocytes of complementary idiotype can stimulate each other. The corresponding nodes are connected by links.

Idiotypes are represented by bit strings [14] of length d, $\boldsymbol{b}_d\boldsymbol{b}_{d-1}\cdots\boldsymbol{b}_1$ with $\boldsymbol{b}_i \in \{0,1\}$. Ideally, d is chosen such that

*ulrich.behn@itp.uni-leipzig.de

2^d is the size of the potential repertoire. The nodes of the network are labeled by these bit strings. Two nodes v and w are linked if their bit strings are complementary, allowing for up to m mismatches; that is, their Hamming distance is $d_H(v,w) \geqslant d - m$. The corresponding undirected graph is the base graph $G_d^{(m)}$. Each node has the same number of neighbors, $\kappa = \sum_{k=0}^{m} \binom{d}{k}$. It represents the potential idiotypic repertoire with all possible interactions.

The bit strings are thought to represent neither the genetic code nor the primary structure (strings of amino acids) of the antibodies. They caricature the phenotype of the antibody's binding sites and provide an easy notion of complementarity [15].

Not all idiotypes are expressed in the real network. In our minimalistic model we only account for whether an idiotype is present or not, correspondingly the node is occupied, $n(v) = 1$, or empty, $n(v) = 0$. The subgraph of $G_d^{(m)}$ induced by the occupied nodes represents the expressed idiotypic network at a given time.

We describe the temporal evolution in discrete time. The influx of new idiotypes from the bone marrow is modeled by occupying empty nodes with probability p [16]. For survival a B lymphocyte needs stimulation by complementary structures. The number of cross-linked receptors determines the strength of stimulation, the response. It is a nonmonotonous function of the concentration of complementary structures, the dose. If their concentration is too high, cross-linking becomes less likely due to steric hindrance, and the response is reduced. The dose-response curve is log-bell shaped (cf. [17] and Refs. therein). In our model an occupied node survives if the number of occupied neighbors is between two thresholds, t_L and t_U. The rules of parallel update are as follows.

(i) Occupy empty nodes with probability p.

(ii) Count the number of occupied neighbors $n(\partial v)$ of node v. If $n(\partial v)$ is outside the window $[t_L, t_U]$, set the node v empty.

(iii) Iterate.

All three, the random and the deterministic steps and the iteration, are equally important [18]. Driven by the random influx of new idiotypes the network evolves towards a quasistationary state of nontrivial, functional architecture in which groups of nodes can be identified according to their statistical properties. Crucial for that is that, besides the random occupation of empty nodes, occupied nodes are emptied if linked with too few or too many occupied nodes.

The paper is organized as follows. In the next section we discuss the model in its scientific context in other disciplines and its relation to other models of idiotypic networks. In Sec. III we provide simulation results. We sketch a typical random evolution of the system to make the reader familiar with the systems behavior. Considering global and local network characteristics the existence of groups of nodes which share statistical properties [13] is confirmed and more details are revealed. In Sec. IV we describe certain regularities in the bit strings of nodes which belong to the same group. The observed patterns can be constructed from pattern modules [19]. The construction principle is explained first for the simplest pattern and generalized afterwards. These findings make it possible to calculate the number of groups, the group sizes, and the linking between groups. A new observable, the center of mass, is introduced, which proves very useful in real-time pattern identification. In Sec. V we apply this concept considering specific patterns observed in simulations, among them a dynamic pattern with core groups, peripheral groups, stable holes, and singletons that resembles in some aspects the biological network [5,6]. In the Appendix we calculate the scaling of the relative size of these groups for systems of biological size.

II. CONTEXT AND RELATED MODELS

The topic falls into several scientific disciplines. It is natural to place our investigations in the context of network theory. Network theory has applications in a plethora of different, multidisciplinary fields [20–22] and has received great attention in the community of statistical physicists in the last decade.

A major body of research deals with growing networks, where new nodes are attached to the existing nodes randomly, or depending on properties of the existing nodes. In this context deletion of nodes is only considered to study the resilience of the network against random or targeted attacks [23]. For recent reviews, see [24–26]; cf. also [21,27].

Natural networks, however, do not grow without limit but stay finite and evolve towards a functional architecture. There are several modes to enable evolution: (i) adding nodes but keeping the growth balanced by deletion [28–33] or merging of nodes [34–36]; (ii) keeping the nodes unaffected but adding, deleting, or reorganizing the links [37–42]; (iii) addition and deletion of both nodes and links [43–49]. Again, this can be done randomly or depending on the properties of the nodes and its neighbors.

Generic observables to characterize networks include the degree distribution, centrality, betweenness, cliquishness, modularity, clustering coefficients, and diameter. For instance, growing networks using preferential attachment have a power law degree distribution like many real world networks. However, the characteristic exponent of preferential attachment networks is larger than the one found in natural networks. This was a major motivation to study evolving networks.

In many natural networks nodes have individual properties which control their potential linking. Clearly, in our case this is the idiotype. Also protein networks, transcription networks, and generally signaling networks belong to this class.

Nodes may have an internal state which can change depending on their neighborhood in the network or on external influences. This dynamics has a typical time scale that is shorter than the time scale for evolution of the network's architecture. The interplay of these processes came into the focus of research only in the last few years. For a recent review and a status report, see [50,51]. Our model is a very early example where this interplay is studied [13]. In the present paper we describe the building principles of the architecture.

Our network model is a Boolean network [52], since each node can be only in one of two states: empty or occupied. The nodes are updated in consecutive time steps depending on its own and its neighborhood occupation.

The model is also a *cellular automaton*; for a comprehensive monograph, see [53]. More precisely, since the update depends only on the sum of the neighbor states and the

state of the node itself, it is a *totalistic* cellular automaton. Cellular automata naturally involve unoccupied nodes. In our model unoccupied nodes, holes, play an important role. We distinguish holes that could be occupied from stable holes, which cannot be occupied due to overstimulation. A simple network picture disregards nodes which are not occupied.

A famous example of a totalistic two-dimensional deterministic cellular automaton is Conway's Game of Life [54]. Both the survival of an occupied cell and the occupation of an empty cell are governed by window rules. Many interesting patterns, depending on the initial conditions—static or dynamic—have been described in detail and classified. The Game of Life was transferred to a variety of lattices, for example, to three-dimensional cubic lattices [55,56], to triangular, pentagonal, and hexagonal tesselations, to Penrose tilings [56–58], and to small world geometry [59]. Larger than Life [60–62] increases the radius of the neighborhood. Also, a probabilistic version on a two-dimensional square lattice has been proposed, where stochastic deviations from the deterministic update are permitted [63]. The mean occupation of cells, a global order parameter, undergoes a sharp phase transition for increasing strength of stochasticity. On the occasion of the 40th anniversary appeared a comprehensive collection of recent results on the Game of Life and its descendants [64]. Our model can be considered as a further version of the Game of Life on a high dimensional graph, where empty nodes are randomly occupied, while the survival of occupied nodes is governed by a deterministic window rule. Starting from an empty graph we observe an evolution toward a complex, highly organized architecture. The model can also be categorized as a stochastic, nonlinear dynamical system.

There exists a variety of models for B-cell networks. References [9,17] give comprehensive surveys of modeling approaches.

For instance, Stewart and Varela [65,66] proposed a model which also has a random influx and a window update rule to simulate the internal dynamics and a zero/one clone population. However, while we consider a discrete d-dimensional hypercubic shape space, in their model the complementary idiotypes live on different sheets of a two-dimensional continuous shape space [67]. A summary of results obtained in models with continuous shape space is given by Bersini [68]. Several aspects of modeling in continuous and discrete shape space are discussed in [69].

An early network model inspired by spin glass physics was proposed by Parisi [70] to describe immunological memory. The interaction between idiotypes in the model of Barra and collaborators [71–73] is also taken from spin glass physics. Their model describes a given number of idiotype populations each with a constant number of lymphocytes. Each cell can be in a firing or quiescent state. The strength of the ferromagnetic coupling between the idiotypes (also encoded by bit strings) models the affinity, which is related to the complementarity of the bit strings. Barra and Agliari [71,72] compute the degree distribution, the type and number of loops, and consider the scaling behavior. They describe primary and secondary immune responses and understand low and high dose tolerance as a network phenomenon. In our model the log-bell-shaped response is integrated as a B-cell property [6,17]. Essential for our approach is a random influx of new cells and a selection mechanism. Hence, we can describe the evolution of the network towards a functional architecture.

A model which distinguishes between antibody molecules and lymphocytes with a dynamics including an influx similar to ours is proposed by Ribeiro *et al.* [74]. They compare the dynamics on given architectures of random and scale-free networks.

IMMSIM, invented by Celada and Seiden [75,76], is also a modified cellular automaton. It incorporates many immunologic agents, including antigen presenting cells, B cells, T cells, antigens, antibodies, and cytokines. It describes both humoral and cellular responses. Idiotypes are also characterized by bit strings. The vast amount of interacting agents increases drastically the number of parameters. The model is intended to be as realistic as possible and to provide experimental and practical immunologists with a tool to test hypotheses *in silico*. Our approach is in a sense complementary. We aim at an understanding of the principles governing the autonomous evolution toward a functional architecture. Therefore, we investigate a minimalistic model with a small number of parameters, which nevertheless exhibits essential features of the biological network.

The concept of idiotypic networks inspired applications in computer sciences, for example, artificial immune systems for the detection of the intrusion of spam or viruses [77,78].

III. SIMULATION RESULTS

In this section we report on simulations on the base graph $G_{12}^{(2)}$, which consists of $2^{12} = 4096$ nodes, each of which has $\kappa = 79$ links to other nodes. The window rule parameters are $[t_L, t_U] = [1, 10]$. The lower threshold is biologically motivated; a node needs at least one occupied neighbor to survive. The upper threshold is chosen to enable a nontrivial, dynamic pattern of complex architecture. As discussed below in more detail, higher t_U would allow a broader variety of static patterns. However, the concept developed in this paper still applies.

All patterns discussed in the following refer to the system's state after application of the window rule, when the system is more ordered than after the next influx.

The simulations start with an empty base graph. The influx p varies from 0 to 0.11. This covers the range in which we find interesting patterns; above $p \gtrapprox t_U/\kappa = 0.127$ there is only trivial random behavior. Obviously, for $p \gg t_U/\kappa$ the occupation of the graph, after application of the window rule, tends to zero.

A. Random evolution

We start the simulations with an empty base graph occupying nodes with probability p. In the first time step only those nodes survive which have at least one occupied neighbor (having more than t_U occupied neighbors is unlikely in the beginning). The surviving nodes represent seeds, the neighbors of which will survive if occupied. Hence, we observe a rapid growth of a giant cluster until more and more nodes have more than t_U occupied neighbors. Exceeding the upper threshold deletes a node. Thus, the giant cluster decays and many stable holes are created, that is, nodes with the number of occupied

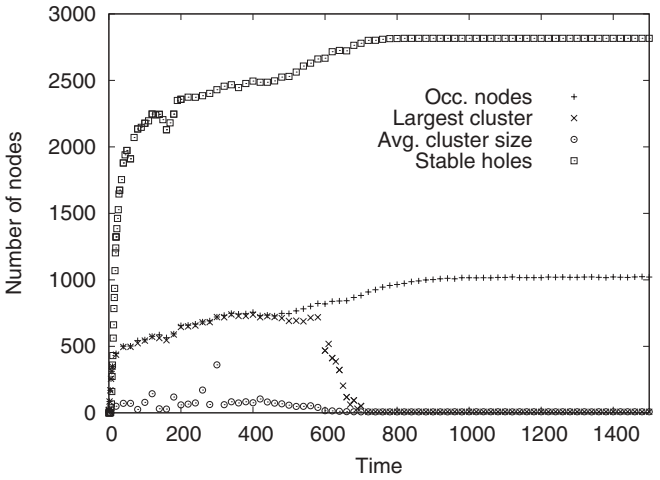

FIG. 1. Time series of the number of occupied nodes $n(G)$, the size of the currently largest cluster $|C^{\max}|$, the average cluster size $\langle |C| \rangle_{\mathcal{C}}$, and the number of stable holes $h^*(G)$ on the base graph $G_{12}^{(2)}$ with $[t_L, t_U] = [1,10]$ and $p = 0.01$. The system evolves to a stationary eight-cluster pattern.

neighbors above the upper threshold t_U. Figure 1 shows a time series for the evolution to a stationary state where the number of stable holes increases up to its stationary value.

The empty base graph is a highly symmetric object. Due to the random influx the symmetry is broken and the system falls into a network configuration of lower symmetry. The typical result of the evolution is a quasistationary pattern of mutually dependent occupied nodes and stable holes. Properly situated occupied nodes create stable holes and in return stable holes in the neighborhood of an occupied node may prevent its overstimulation.

In the generic case for a given p a certain pattern type is found most frequently. Occasionally, depending on the history of the driving process, also other patterns occur. Once established, they all can live for a long time. (This can be proved in simulations preparing the pattern as initial configuration.)

In principle, the system is ergodic [79]. This becomes immediately clear considering the following unlikely but possible event. For any choice of $p > 0$ the occupation of nodes by the influx can be such that the application of the window rule leads to an empty base graph. After this extinction catastrophe the further realization of the driving process, the influx, determines to which pattern the system evolves. For any $p > 0$ an infinite trajectory contains partial trajectories leading to any possible pattern. In practice, in our simulations we have never seen such an extinction catastrophe but only quasistationary patterns usually living for a long time. For increasing system size such catastrophes become less likely. In the thermodynamic limit we expect a breaking of ergodicity.

In our finite system there can be transitions between different patterns on a route without extinction catastrophe but via the formation of an intermediate, unstable giant cluster (for more details, see [13]).

Modeling biological systems we should keep in mind that they are finite and have a finite life expectation. The quasistationary state could persist for times longer than the life span of the individual but transitions between different states cannot be excluded. Moreover, the parameters could vary during the individual's life.

B. Global characteristics

A first characterization of the different patterns can be obtained considering global quantities. They include the number of occupied nodes on the base graph

$$n(G) = \sum_{v \in G} n(v), \tag{1}$$

where $n(v) \in \{0,1\}$ is the occupation of node v, the size of the largest cluster in the set of present clusters $\mathcal{C}$,

$$|C^{\max}| = \max_{C \in \mathcal{C}} (|C|), \tag{2}$$

and the average size of the clusters,

$$\langle |C| \rangle_{\mathcal{C}} = \frac{1}{N_C} \sum_{C \in \mathcal{C}} |C|, \tag{3}$$

where N_C is the current number of clusters and $\langle \cdot \rangle_{\mathcal{S}}$ denotes the average over the elements of some set $\mathcal{S}$. Clusters, that is, connected parts of the occupied subgraph, are very characteristic for patterns. Finally, we mention the number of stable holes $h^*(G)$, that is, empty nodes with $n(\partial v) > t_U$.

Figure 1 shows a generic time series of these global characteristics for a parameter setting where the system evolves to a stationary eight-cluster pattern.

In the stationary state we can consider temporally averaged global quantities. The temporal average is defined as

$$\overline{x} = \frac{1}{T_1 - T_0} \sum_{t \in (T_0, T_1]} x_t, \tag{4}$$

where T_0 should be larger than the relaxation time in which the system reaches the stationary state, and $(T_0, T_1]$ is the averaging period.

Table I gives results for three patterns which occur for different influx p. The static patterns are named according to the size of the characteristic clusters. With a deeper understanding of the architecture we name them by the number of groups of nodes; see Sec. IV below.

The eight-cluster pattern at $p = 0.005$ has 128 clusters of size 8, which results in a total average population of 1024 occupied nodes, that is, one-fourth of all nodes. The remaining nodes are holes, 2816 of which are stable $[n(\partial v) > t_U]$ and 256 are not stable $[n(\partial v) \leqslant t_U]$. Empty nodes with $n(\partial v) < t_L$ are not counted as stable holes, since they could easily become

TABLE I. Temporal averages and standard deviations of global characteristics for three typical patterns. Data from 500 000 iterations.

Pattern	Eight-cluster	Two-cluster	Dynamic
p	0.005	0.015	0.025
$\overline{n(G)}$	1024.6 ± 0.8	1023.3 ± 0.9	533.4 ± 27.7
$\overline{h^*(G)}$	2816.0 ± 0.0	3055 ± 20	1828 ± 114
$\overline{\lvert C^{\max} \rvert}$	8.0 ± 2.8	4.5 ± 2.1	410 ± 20
$\overline{\langle \lvert C \rvert \rangle_{\mathcal{C}}}$	7.96 ± 0.04	2.01 ± 0.01	4.49 ± 0.96
$\overline{N_C}$	128.6 ± 0.8	510.4 ± 3.7	123.1 ± 22.0

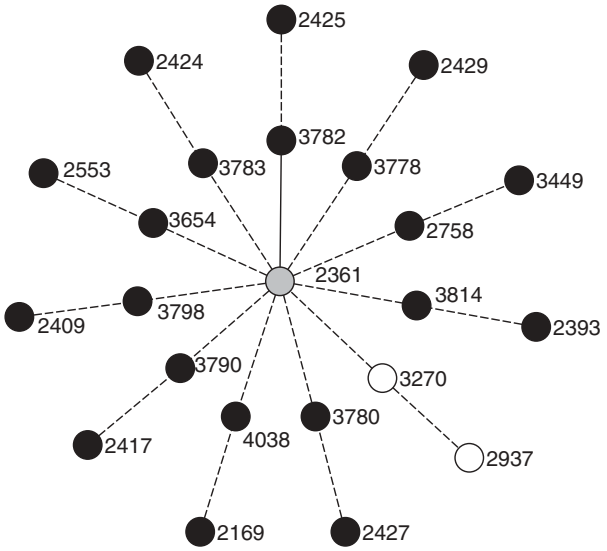

FIG. 2. Hub in the two-cluster pattern. A defect, an unoccupied two cluster (open circles), in the perfect two-cluster pattern allows the occupation of a node (gray) which connects ten occupied two clusters (black). Defects are rare and an occupied hub will not survive the next update if one of its empty neighbors, for example, of the missing two cluster, becomes occupied. There is one link (solid line) with one mismatch, the other links (dashed lines) have two mismatches. The nodes are labeled with the decimal expressions of their bit strings. Figure produced using yEd [80].

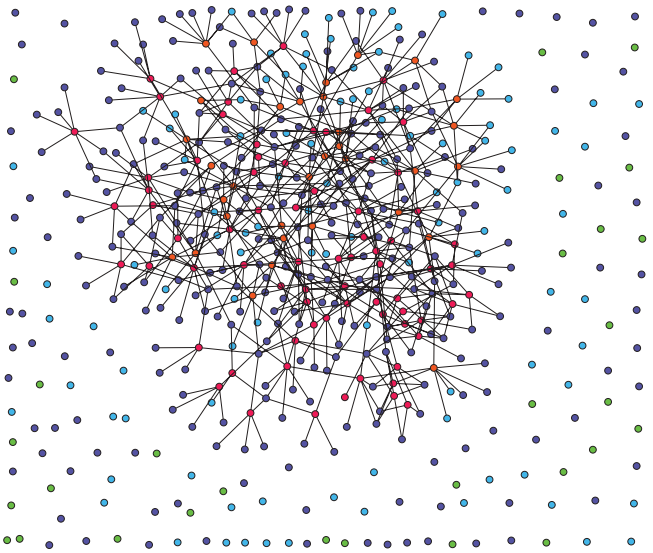

FIG. 3. (Color online) Snapshot of the occupied graph of the complex configuration of a dynamic pattern for $p = 0.025$. As an additional information, the nodes are colored according to their membership in different groups [see Fig. 15 (top)]; nodes within a group have similar statistical characteristics (see text). Figure produced using yEd [80].

occupied and sustained by the random influx. Figure 1 shows the temporal evolution from an empty base graph towards an eight-cluster pattern.

In the two-cluster pattern at $p = 0.015$ the 510 clusters of size 2 together occupy about one-fourth of the base graph. The remaining three-quarters are stable holes. Defects in the perfect two-cluster pattern allow that occasionally some of the node pairs become connected via a central hub and a larger star-shaped cluster is formed (see Fig. 2). $t_U = 10$ was chosen to exclude the occupation of the hub in the perfect pattern. Both the eight- and the two-cluster patterns are quasistatic; the temporal fluctuations are small.

A more complex, dynamic pattern evolves for larger $p \gtrapprox 0.03$. The standard deviation of the temporal averages is one order of magnitude larger than in the two static patterns. Figure 3 shows a snapshot of the occupied graph. We see one large cluster of about 400 nodes and about 120 isolated nodes. These nodes had at least one occupied neighbor which was removed in latest update. Further, approximately 1800 stable holes and 1800 unstable holes have been observed, which are not shown in the figure. We can clearly distinguish a central and a peripheral part, which are supposed to be of functional importance in the biological idiotypic network.

C. Local characteristics

Besides global quantities, time averages of local quantities characterizing every single node can be considered. Elucidating are the mean occupation $\overline{n}(v)$, the number of occupied neighbors $\overline{n}(\partial v)$, and the mean lifetime $\overline{\tau}(v)$, which is defined as

$$\overline{\tau}(v) = \frac{1}{b(v) + n_{T_0}} \sum_{t \in (T_0, T_1]} n_t(v), \tag{5}$$

where $b(v)$ is the number of births during the observation time, that is, the number of new occupations of the node by the influx. Of course, $b(v) + n_{T_0} \neq 0$ must be fulfilled; otherwise $\overline{\tau}(v)$ has no meaning.

We can identify groups of nodes sharing statistical properties as proposed in [13]. Figure 4 shows mean occupation, mean lifetime, and the number of occupied neighbors vs influx probability. The groups appear as peaks in the histograms. The number of occupied neighbors proves most suitable to distinguish the different groups.

For small and moderate influx a clear group structure is visible. The data for the mean lifetime and the mean occupation suggest that the patterns are static for $p \lessapprox 0.03$. These patterns have groups of occupied nodes with a high mean lifetime; other groups are stable holes or sparsely occupied nodes. For $0.03 \lessapprox p \lessapprox 0.08$ the patterns are dynamic, but still stationary. Also in dynamic patterns there are stable holes. The mean lifetime of occupied nodes is small; the occupied subgraph changes continuously. While in static and dynamic patterns all nodes remain in their groups, for high influx $p \gtrapprox 0.08$ the patterns become short-lived; groups dissolve and reemerge in a different configuration. Their distinction by temporal averages becomes more and more difficult. For very high influx $p \gg 0.12$ the dynamics is entirely random.

IV. CONCEPT OF PATTERN MODULES

We find regularities in the bit strings encoding nodes belonging to the same group. This makes it possible to identify general building principles. Patterns are built from

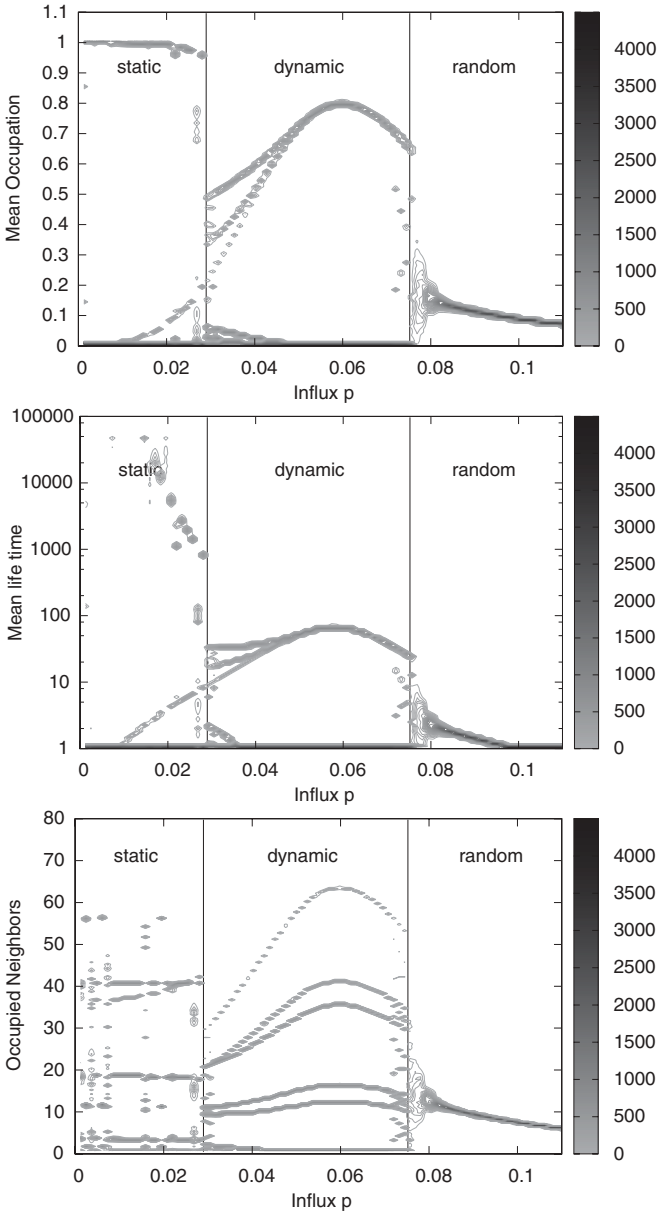

FIG. 4. Time averages of the mean occupation (top), the mean lifetime (center), and the mean number of occupied neighbors (bottom) of each node for increasing values of p, $\Delta p = 5/4096$. Each graph shows isolines of a histogram in the top view. The gray scale reflects the number of nodes with the corresponding property. Regimes of different temporal behaviors are separated by vertical lines. For each p data is from time series of 500 000 iterations in the stationary state, starting from an empty base graph $G_{12}^{(2)}$.

more elementary objects, so called *pattern modules*. With this concept we can derive all structural properties, the size of the groups and their linking, of the patterns observed so far in the simulations.

We first explain the principles on the example of the two-cluster pattern and develop then the detailed concept for the general case. At the end of the section, exploiting this concept, we introduce the center of mass vector, a tool which makes it possible to identify in simulations the majority of patterns in real time.

A. Simplest case: The two-cluster pattern

We introduce the building principles of patterns considering the simplest pattern, the two-cluster pattern which appears for moderate influx. In simulations starting from empty base graphs it is rare and only found for $0 < p \lessapprox 0.03$, but if prepared as initial condition it is very stable for a larger range of p up to 0.045. By their statistical characteristics (cf. Table II) we can distinguish three groups of nodes, frequently *occupied nodes* (S_1) with a high mean lifetime, permanently empty *stable holes* (S_3), and rarely occupied *potential hubs* (S_2), which link together up to t_U two clusters if occupied.

Looking at the node indices i_v in decimal representation we observed that the sum of the two indices in a two cluster is constant in a realization. In a different realization the index sum can be different. For instance, in Fig. 2 the index sum within all two clusters is 6207. This indicates regularities at the level of the bit strings.

We found that all occupied nodes are identical in exactly two bits, say at position k and l. The members of a two cluster are complementary in all other bits; in symbols we write

$$\cdots \boldsymbol{b}_k \cdots \boldsymbol{b}_l \cdots \quad \text{is linked with} \quad \overline{\cdots \boldsymbol{b}_k \cdots \boldsymbol{b}_l \cdots},$$

where the bar denotes the bit inversion. The bit strings of all stable holes are also equal in the same two bit positions k and l. However, they are inverse to $\boldsymbol{b}_k$ and $\boldsymbol{b}_l$ of the occupied nodes. Potential hubs have exactly one inverse and one equal bit in these positions. As these bits play a crucial role, we call them *determinant bits*. The regularities are summarized by

$$\begin{aligned} &\text{occupied nodes } S_1 && \cdots \boldsymbol{b}_k \cdots \boldsymbol{b}_l \cdots, \\ &\text{potential hubs } S_2 && \begin{cases} \cdots \overline{\boldsymbol{b}_k} \cdots \boldsymbol{b}_l \cdots, \\ \cdots \boldsymbol{b}_k \cdots \overline{\boldsymbol{b}_l} \cdots, \end{cases} \\ &\text{stable holes } S_3 && \cdots \overline{\boldsymbol{b}_k} \cdots \overline{\boldsymbol{b}_l} \cdots. \end{aligned}$$

The example in Fig. 2 has the determinant bits in positions 7 and 12, $\boldsymbol{b}_7 = \boldsymbol{b}_{12} = 1$.

This makes it possible to explain all structural properties of the pattern observed in the simulations. We can construct an ideal two-cluster pattern, a configuration in which all nodes of group S_1 are occupied and the others remain empty. It is ideal in the sense that there are no defects but also no hubs.

Since all other bits can take all possible combinations, the size of the groups can be calculated; for example, there are $|S_1| = 2^{d-2}$ occupied nodes and $|S_2| = 2 \times 2^{d-2}$ potential hubs.

We further can compute the number of occupied neighbors $n(\partial v)$ of a node v of any group. Since all nodes of S_1 are occupied in the ideal pattern, $n(\partial v)$ is given by the number of

TABLE II. Local characteristics of the three groups in the two-cluster pattern for $p = 0.025$ compared with the ideal pattern. Data from a time series of 500 000 iterations.

		S_1	S_2	S_3
Mean occupation	$\langle \overline{n}(v) \rangle_{S_i}$	0.993	0.0004	0.000
	n_{ideal}	1	0	0
Occupied neighbors	$\langle \overline{n}(\partial v) \rangle_{S_i}$	1.002	10.95	55.64
	$n(\partial v)_{\text{ideal}}$	1	11	56
Mean lifetime	$\langle \overline{\tau}(v) \rangle_{S_i}$	6923	0.016	0.000

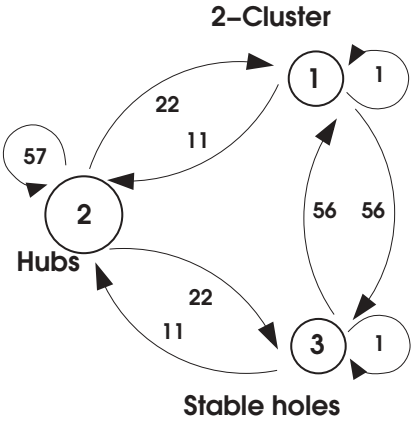

FIG. 5. The three groups of the two-cluster pattern and their linking. The circle sizes correspond to the group sizes. The arrows and the numbers next to them indicate how many nodes of a group exert influence on the nodes of another group, for example, each node of S_2 is stimulated by 11 nodes from S_1. The number of links can be counted in simulations or taken from the link matrix that is derived in Sec. IV B.

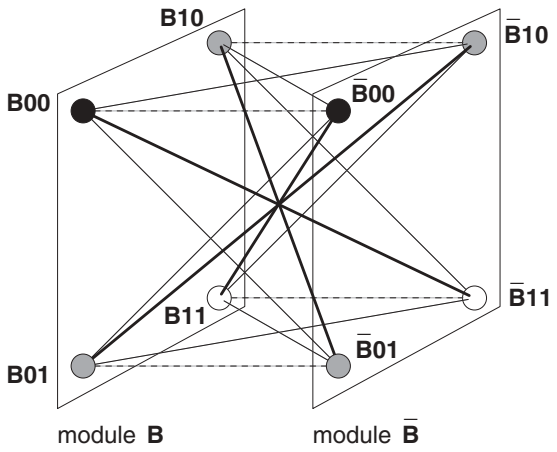

FIG. 6. Two pattern modules with complementary nondeterminant bit chains B and $\overline{\mathsf{B}}$, respectively, on a two mismatch base graph with a two-cluster configuration. The two-dimensional modules are congruently occupied, each consisting of one occupied node (black, **·00**), two potential hubs (gray, **·01** and **·10**) and one stable hole (white, **·11**). The positions and values of the determinant bits are chosen without loss of generality. The links have no mismatch (bold lines), one (solid lines), or two mismatches (dashed lines). There are 2^{d-2} pattern modules, each pair of which with complementary nondeterminant bits contribute a pair of occupied nodes.

links between v and nodes in S_1. A link between two nodes exists if their bit strings are complementary except for up to two mismatches. If $v \in S_1$, it has two bits in common with all other nodes in S_1, namely $\boldsymbol{b}_k$ and $\boldsymbol{b}_l$. Thus, all remaining bits must be exactly complementary. There is only *one* node $w \in S_1$, which obeys this constraint. If $v \in S_2$ or $v \in S_3$, there is one predetermined mismatch or none, respectively. The remaining mismatches can be distributed among the $d-2$ nondeterminant bits. Thus, a node in S_i has

$$n(\partial v)_{\text{ideal}} = \sum_{j=0}^{i-1} \binom{d-2}{j} \tag{6}$$

occupied neighbors in the ideal pattern. For small influx this is in good agreement with the simulations (cf. Table II). In a similar way for all nodes the number of links to nodes in different groups can be calculated; the result is visualized in Fig. 5. The derivation for the general case is given in the next section.

This regularity encouraged the following concept. Considering the two determinant bits as coordinates of a two-dimensional space, they define the corners of a two-dimensional hypercube. The corner with coordinates $(\boldsymbol{b}_k, \boldsymbol{b}_l)$ represents an occupied node, the opposite corner $(\overline{\boldsymbol{b}_k}, \overline{\boldsymbol{b}_l})$ is a stable hole, and the neighboring corners of $(\boldsymbol{b}_k, \boldsymbol{b}_l)$ are potential hubs. We call this structure a *pattern module*, because it is the building block for the entire regular configuration. In a different picture, we can also understand an ideal configuration as consisting of 2^{d-2} congruently occupied "parallel worlds." Figure 6 illustrates the concept of pattern modules.

Any choice of the two determining bits is of course possible, all corresponding patterns are equivalent, the two-cluster pattern is $2^2 \times \binom{d}{2}$-fold degenerated, where the first factor represents the choice of the two determinant bits, and the second factor gives the number of possible positions of these bits in the bit string of length d . It is the individual history (the realization of the random influx) which selects the determining bits and thus breaks the symmetry.

The two-cluster pattern consists of idiotype–anti-idiotype pairs which mutually stimulate each other. In such a pair the anti-idiotypic clone carries the internal image of an antigen which the idiotypic clone is able to recognize, and vice versa. However, the pattern as a whole is a regular array of two clusters with two-mismatch links. It is organized in such a way that every empty node has occupied neighbors. An antigen inserted in an empty node will be surely recognized. In this sense the pattern is complete, but it has no place for self. In addition, the pattern is essentially static and therefore not adaptive.

B. General case

1. Groups

Many results for two-cluster patterns on the $G_{12}^{(2)}$ base graph can be generalized to more complex architectures and other choices of d and m. This includes the eight-cluster pattern mentioned in Sec. III and other static patterns as well as the dynamic pattern. Their structure is correctly described by pattern modules with more than two determinant bits.

In the same way as for the two-cluster pattern, we define the pattern module as a hypercube of dimension d_M, where d_M is the number of determinant bits. There are two groups which are represented by only one node in the pattern module. One of them is labeled S_1. All nodes in group S_1 have the same determinant bits $\boldsymbol{b}_1 \cdots \boldsymbol{b}_{d_M}$. The other groups are ordered such that the determinant bits of S_j differ in $j-1$ positions from the determinant bits of S_1. It is clear that there are $d_M + 1$ groups. Groups S_j and S_{d_M+2-j} are equivalent; they have the same size and linking properties (see below). In typical patterns,

occupation breaks the symmetry. We usually label the smallest group of the more occupied half as S_1, which is, of course, arbitrary.

The size of the groups can be obtained by elementary combinatorics. Since the ith group deviates in $i-1$ out of d_M determinant bit positions of S_1, there are $\binom{d_M}{i-1}$ choices. This number is multiplied by the number of pattern modules on the base graph given by 2^{d-d_M}. The group size is

$$|S_i| = 2^{d-d_M}\binom{d_M}{i-1}, \quad i = 1,\ldots,d_M+1. \tag{7}$$

The factor $\binom{d_M}{i-1}$ is called the relative group size, since it is the group size normalized by the size of S_1. It is independent of the base graph dimension d and the number of mismatches m.

As an example, we can construct two-cluster patterns on a base graph $G_d^{(m)}$ by means of pattern modules with exactly one occupied node (S_1). The dimension of the pattern module d_M then has to equal the number of allowed mismatches m. The number of qualitatively distinguishable groups is $m+1$, etc. A two-cluster pattern can emerge if the lower threshold is $t_L \leqslant 1$ and the upper threshold obeys $1 \leqslant t_U \leqslant d-m$. The two-cluster pattern on one-mismatch graphs described in [13] is an instance of such a pattern. However, in the one-mismatch case one half of all nodes are occupied; the other half are stable holes.

2. Linking

Each node on $G_d^{(m)}$ has $\kappa = \sum_{k=0}^{m}\binom{d}{k}$ links, κ is constrained by the allowed number of mismatches m. We consider a pattern with d_M determinant bits. Each node in group S_i is linked to L_{ij} neighbors in group S_j. The L_{ij} are the entries of the link matrix $\mathbb{L}$. $\mathbb{L}$ defines the architecture of a pattern built of modules of dimension d_M.

The dynamics of a node depends on the number of occupied neighbors. The mean occupation is a typical common property of nodes belonging to the same group. Thus, the knowledge of the group membership of the node's neighbors is of crucial importance to understand its statistical properties.

Within the concept of pattern modules $\mathbb{L}$ can be derived combinatorially. Recall that the determinant bit string of a node in S_l deviates in $l-1$ bits from the determinant bit string of a node v_1 in S_1. In the following we consider a node $v^{(i)}$ chosen such that the $i-1$ bits inverse to the corresponding bits of v_1 are left-aligned; its nondeterminant bits are denoted by B. This choice is without loss of generality, because all the arguments do not depend on the labeling of the bit position. From the nodes in S_j we choose $v^{(j)}$ such that the $j-1$ bits inverse to the corresponding bits of v_1 are right-aligned and the nondeterminant bits are $\overline{\mathsf{B}}$. There is no other node in S_j with fewer mismatches to $v^{(i)}$.

We have to distinguish whether the partial bit strings of length $i-1$ and $j-1$ do overlap. These cases are discriminated by the value of $\Delta_{ij} = d_M - i - j + 2$. There are three cases.

(i) $\Delta_{ij} = 0$. All determinant bits of $v^{(i)}$ and $v^{(j)}$ are complementary.

(ii) $\Delta_{ij} > 0$. $v^{(i)}$ and $v^{(j)}$ share Δ_{ij} determinant bits with v_1. This case is illustrated as

$$\begin{array}{lcccc} v_1 & \boldsymbol{b}_1 \ldots \boldsymbol{b}_{i-1} & \boldsymbol{b}_i \ldots \boldsymbol{b}_{d_M-j+1} & \boldsymbol{b}_{d_M-j+2} \ldots \boldsymbol{b}_{d_M}, \\ v^{(i)} & \overline{\boldsymbol{b}_1 \ldots \boldsymbol{b}_{i-1}} & \boldsymbol{b}_i \ldots \boldsymbol{b}_{d_M-j+1} & \boldsymbol{b}_{d_M-j+2} \ldots \boldsymbol{b}_{d_M}, \\ v^{(j)} & \underbrace{\boldsymbol{b}_1 \ldots \boldsymbol{b}_{i-1}}_{i-1 \text{ bits}} & \underbrace{\boldsymbol{b}_i \ldots \boldsymbol{b}_{d_M-j+1}}_{\Delta_{ij}=d_M-i-j+2 \text{ bits}} & \underbrace{\overline{\boldsymbol{b}_{d_M-j+2} \ldots \boldsymbol{b}_{d_M}}}_{j-1 \text{ bits}}. \end{array}$$

(iii) $\Delta_{ij} < 0$. $v^{(i)}$ and $v^{(j)}$ share $|\Delta_{ij}|$ determinant bits which are inverse to the corresponding bits of v_1, see diagram below:

$$\begin{array}{lcccc} v_1 & \boldsymbol{b}_1 \ldots \boldsymbol{b}_{d_M-j+1} & \boldsymbol{b}_{d_M-j+2} \ldots \boldsymbol{b}_{i-1} & \boldsymbol{b}_i \ldots \boldsymbol{b}_{d_M}, \\ v^{(i)} & \overline{\boldsymbol{b}_1 \ldots \boldsymbol{b}_{d_M-j+1}} & \overline{\boldsymbol{b}_{d_M-j+2} \ldots \boldsymbol{b}_{i-1}} & \boldsymbol{b}_i \ldots \boldsymbol{b}_{d_M}, \\ v^{(j)} & \underbrace{\boldsymbol{b}_1 \ldots \boldsymbol{b}_{d_M-j+1}}_{i-1 \text{ bits}} & \underbrace{\boldsymbol{b}_{d_M-j+2} \ldots \boldsymbol{b}_{i-1}}_{-\Delta_{ij}=i+j-d_M-2 \text{ bits}} & \underbrace{\boldsymbol{b}_i \ldots \boldsymbol{b}_{d_M}}_{d_M-i+1 \text{ bits}}. \end{array}$$

The number of mismatches between $v^{(i)}$ and $v^{(j)}$ is $|\Delta_{ij}|$. If $|\Delta_{ij}| \leqslant m$ there is a link between $v^{(i)}$ and $v^{(j)}$. In this case there are further nodes in S_j which link to $v^{(i)}$, the number of which is calculated combinatorially. There are $m - |\Delta_{ij}|$ additionally allowed mismatches which can appear among nondeterminant and/or determinant bits.

In cases (ii) and (iii) there are further nodes in S_j with $|\Delta_{ij}|$ mismatches to $v^{(i)}$. These are obtained by distributing the $|\Delta_{ij}|$ mismatches among the $d_M - i + 1$ right-aligned bits in case (ii), or among the $i-1$ left-aligned bits in case (iii). This leads to $\binom{d_M-i+1}{\Delta_{ij}}$ and $\binom{i-1}{|\Delta_{ij}|}$ nodes in the respective cases.

Now we consider additional mismatches. Among the $d - d_M$ nondeterminant bits we can distribute l mismatches in

$$\binom{d-d_M}{l}$$

different ways.

Among determinant bits additional mismatches can only appear in pairs. This is relevant for $m - |\Delta_{ij}| \geqslant 2$. If we invert one bit in $v^{(j)}$, the resulting node is not in S_j since the number of bits complementary to v_1 is changed. We have to invert a second bit so that the number of mismatches with v_1 remains constant. The number of nodes in S_j with $|\Delta_{ij}| + 2k$ mismatches to $v^{(i)}$ is computed as follows.

In case (ii) we invert k bits in the $i-1$ left-aligned bits of $v^{(j)}$. There are $\binom{i-1}{k}$ possibilities. To compensate for this, we have to invert k bits among the $j-1$ right-aligned bits of $v^{(j)}$. Altogether, there are now $\Delta_{ij} + k$ mismatches to $v^{(i)}$ living on the $d_M - i + 1$ right-aligned bits. There are $\binom{d_M-i+1}{\Delta_{ij}+k}$ possibilities to distribute them. Thus, we have

$$(i-1k)\binom{d_M-i+1}{\Delta_{ij}+k}$$

nodes in S_j with $\Delta_{ij} + 2k$ mismatches to $v^{(i)}$.

Case (iii) is similar. We invert k bits in the $d_M - i + 1$ right-aligned bits of $v^{(j)}$, there are $\binom{d_M-i+1}{k}$ possibilities. To compensate this, we have to invert k bits among the $d_M - j + 1$ left-aligned bits of $v^{(j)}$. Together, $\Delta_{ij} + k$ mismatches

to $v^{(i)}$ live on the $i-1$ left-aligned bits. There are $\binom{i-1}{|\Delta_{ij}|+k}$ possibilities. This leads to

$$\binom{d_M-i+1}{k}\binom{i-1}{|\Delta_{ij}|+k}$$

nodes in S_j with $|\Delta_{ij}|+2k$ mismatches to $v^{(i)}$.

The result in case (i) is obtained setting $\Delta_{ij}=0$, and the result for redistributing only $|\Delta_{ij}|$ mismatches derived before is reproduced for $k=0$.

Since the total number of mismatches between linked nodes can not exceed m, l and k are constrained by $l+2k+|\Delta_{ij}|\leqslant m$. Summarizing, we obtain for $\Delta_{ij}\geqslant 0$

$$L_{ij}=\sum_{l,k=0}\binom{d-d_M}{l}\binom{i-1}{k}\binom{d_M-i+1}{\Delta_{ij}+k}\times\mathbb{1}(l+2k+\Delta_{ij}\leqslant m), \tag{8}$$

and for $\Delta_{ij}\leqslant 0$

$$L_{ij}=\sum_{l,k=0}\binom{d-d_M}{l}\binom{i-1}{|\Delta_{ij}|+k}\binom{d_M-i+1}{k}\times\mathbb{1}(l+2k+|\Delta_{ij}|\leqslant m). \tag{9}$$

In some cases the evaluation of the sums in Eqs. (8) and (9) leads to simple rules (see [81]).

Of course, the total number of links of a node is

$$\sum_{j=1}^{d_M+1}L_{ij}=\kappa. \tag{10}$$

The link matrix $\mathbb{L}=(L_{ij})$ has a symmetry given by

$$L_{ij}=L_{d_M+2-i,d_M+2-j}. \tag{11}$$

If the link matrix entries of the ith row are multiplied by the size of group S_i, the resulting matrix with entries $\Lambda_{ij}=|S_i|L_{ij}$ additionally obeys $\Lambda_{ij}=\Lambda_{ji}$.

It may be of interest to know the number of links from a node of S_i to nodes of S_j with a given number of mismatches μ, which is denoted by L_{ij}^{μ}. It is obtained replacing in Eqs. (8) and (9) $\mathbb{1}(l+2k+|\Delta_{ij}|\leqslant m)$ by $\delta_{l+2k+|\Delta_{ij}|,\mu}$, which gives, for example, for $\Delta_{ij}\geqslant 0$

$$L_{ij}^{\mu}=\sum_{k}\binom{d-d_M}{\mu-2k-\Delta_{ij}}\binom{i-1}{k}\binom{d_M-i+1}{\Delta_{ij}+k}. \tag{12}$$

Obviously, it holds $L_{ij}=\sum_{\mu=0}^{m}L_{ij}^{\mu}$.

3. *Architecture*

For the link matrix and, thus, for the architecture of patterns we can state a number of general properties. Because $|\Delta_{ij}|=|d_M-i-j+2|\leqslant m$ is the necessary and sufficient condition for the existence of links between groups i and j, all nonzero matrix entries are situated on a band along the secondary diagonal (see the illustration of the general structure of the link matrix in Fig. 7). The width of this band is $2m+1$; that is, m controls the range of influence of a group. Group S_i interacts with the $2m+1$ groups $S_{d_M+2-i-m},\ldots,S_{d_M+2-i+m}$.

We always find groups with self-coupling, because there is always a quadratic block of nonzero matrix entries in the center of $\mathbb{L}$. Such groups are called core groups. The size of the core, that is, the number of core groups, depends on m and on the existence of a central element in $\mathbb{L}$. Such an element exists if d_M is an even number. Thus,

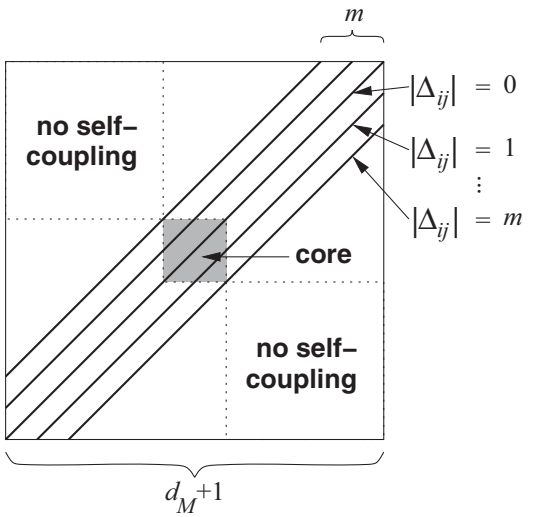

FIG. 7. The general structure of the $(d_M+1)\times(d_M+1)$ link matrix. Matrix entries along the $2m+1$ solid diagonal lines are nonzero [cf. Eqs. (8) and (9)]. All other entries are zero. Groups in the center (gray square) couple to themselves and are naturally called core groups. Among the groups without self-coupling we can further distinguish groups that couple to the core from those which do not. See further discussion in the text.

$$\text{No. of core groups}=\begin{cases}m & \text{if either } m \text{ or } d_M \text{ odd},\\ m+1 & \text{otherwise.}\end{cases} \tag{13}$$

Groups without self-coupling exist if the number of groups d_M+1 is larger than the number of core groups. Such groups are related to the square submatrix of $\mathbb{L}$ with all entries equal to zero (cf. Fig. 7).

The number of core groups for a given m depends only on whether d_M is even or odd but is independent on d. We can represent the content of Fig. 7 in an alternative way exploiting that groups with index i have the same properties as those with index d_M+2-i. In Fig. 8 these groups are on the same position in the two parallel strands. The core groups are on the right end of the diagram. We distinguish two cases, with even and odd number of core groups, respectively, which form the "head" of a caterpillar. If we increase d_M by two, this does not change, but only the "tail" of the caterpillar gains an additional segment. This observation can be used to determine the scaling of the group sizes for large d (cf. the appendix of this paper).

Note that all these general properties in this section are structural information about the patterns. They only depend on the parameters d, m and on the choice of a pattern module d_M.

The above analysis, visualized in Figs. 7 and 8, shows that there always exist core groups which are linked internally and to each other. If the module dimension d_M is large enough, we additionally have peripheral groups linked with the core. For d_M still larger, groups may occur which are not linked to the core. Thus, already on this stage we can say that the model

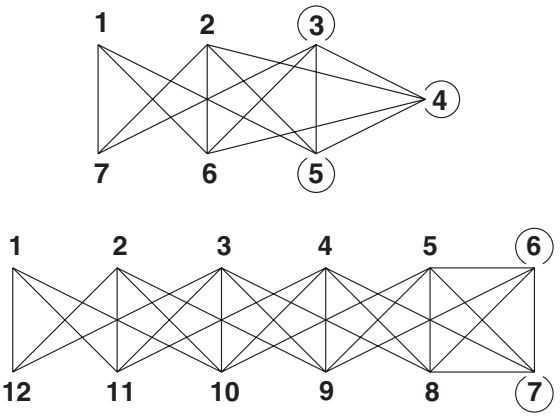

FIG. 8. Groups and their linking for even (top) and odd d_M (bottom) on a two-mismatch base graph. The lines show possible links between nodes of the groups. The circles indicate the self-coupling within the core groups. It is suggestive to call arrangement of the groups caterpillar representation.

has the potential to describe a core-periphery architecture, as proposed in the second generation concept of idiotypic networks [6].

4. Center of mass

In the simulations time series of 2^d nodes are generated, for example, to calculate the mean occupation. In order to identify patterns in real time it has proven useful to reduce this information by introducing—in analogy to classical mechanics—a center of mass vector in dimension d. We consider occupied nodes, $n(v) = 1$, as unit point masses in a d-dimensional space $[-1,1]^d$. The position vector $\boldsymbol{r}(v)$ of a node v encoded by the bit chain $\boldsymbol{b}_d \boldsymbol{b}_{d-1} \cdots \boldsymbol{b}_1$ with $\boldsymbol{b}_i \in \{0,1\}$ has components $r_i(v) = 2\boldsymbol{b}_i - 1$ in this space. The center of mass is defined as

$$\boldsymbol{R} = \frac{1}{n(G)} \sum_v n(v)\boldsymbol{r}(v). \tag{14}$$

The definition of $\boldsymbol{r}(v)$ ensures symmetry with respect to $\boldsymbol{r} = 0$, which implies that for any symmetrically occupied pattern, for example, the completely occupied base graph, we have $\boldsymbol{R} = 0$.

Figure 9 is a typical example of a time series of the d components of $\boldsymbol{R}$. Stationary states are characterized by small fluctuations of the components R_i around some average values $\overline{R}_i$, think, for example, of a moving average. The value of $\overline{R}_i$ makes it possible in the typical case to decide whether i is a determinant bit position.

In general, for all nondeterminant positions i we have $\overline{R}_i \approx 0$. For any choice of determinant bits, the nondeterminant bits run through all combinations of zeros and ones. Therefore, supposing that all nodes within a group are occupied with the same probability, the expected contribution of each group to the nondeterminant components of $\boldsymbol{R}$ is zero.

For patterns which break the symmetry, the R_i for determinant bit positions i are nonzero, positive or negative. We explain in the following example, what can be inferred from this information.

We consider a pattern with $d_M = 4$. Figure 10 shows the determinant bits which contribute to the groups of this pattern.

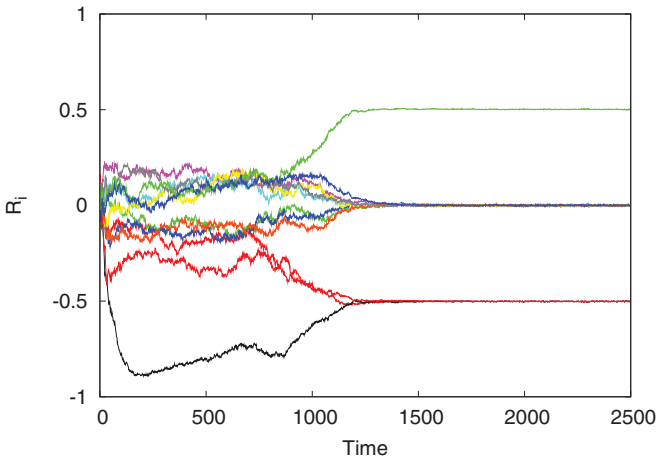

FIG. 9. (Color online) A typical time series of the center of mass vector components, from here on $G_{12}^{(2)}$ with $[t_L,t_U] = [1,10]$ for $p = 0.01$. The evolution starts from an empty base graph, which is gradually occupied, thus breaking the symmetry. A stationary state is reached after about 1300 time steps. Four components fluctuate around nonzero mean values, $R_1, R_7, R_{10} \approx -0.5$, and $R_{11} \approx 0.5$. Hence, as explained in the text, it is an architecture with $d_M = 4$ determinant bits and all nodes in S_1 have $\cdot\mathbf{10}\cdot\cdot\mathbf{0}\cdot\cdot\cdot\cdot\mathbf{0}$. The time series of global quantities in Fig. 1 describes a different realization, which also evolves to a $d_M = 4$ pattern.

Nondeterminant bits are not shown. In S_2 in each bit position the respective bits of S_1 predominate, in S_4 those of S_5 predominate. In S_3 the respective bits of S_1 and S_5 occur with the same frequency (cf. Fig. 10).

For a symmetry breaking pattern where $n(S_1 \cup S_2) > n(S_4 \cup S_5)$, the sign of a determinant component R_i is determined by the corresponding determinant bit $\boldsymbol{b}_i(v_1)$ of a node v_1 in S_1, $\operatorname{sgn} R_i = r_i(v_1) = 2\boldsymbol{b}_i(v_1) - 1$. The other way round, measuring $\operatorname{sgn} R_i$ we can infer $\boldsymbol{b}_i(v_1)$. If $n(S_1 \cup S_2) < n(S_4 \cup S_5)$ we can return to the case above by relabeling the groups. The determinant bits $\boldsymbol{b}_i(v_1)$ of the pattern in Fig. 9 are $\mathbf{0}$ for $i = 1,7,10$ and $\mathbf{1}$ for $i = 11$.

The expectation value $\overline{R}_i$ for a given pattern is easily computed in terms of the expected occupation of the different groups $\overline{n}(S_j)$. For a given j a fraction $(d_M - j + 1)/d_M$ of the occupied nodes contributes $r_i(v_1)$, and a fraction $(j-1)/d_M$ contributes $-r_i(v_1)$. For a determinant bit at position i we obtain

$$\overline{R}_i \approx \left[\frac{1}{\overline{n}(G)} \sum_{j=1}^{d_M+1} \frac{d_M - 2j + 2}{d_M}\, \overline{n}(S_j) \right] r_i(v_1), \tag{15}$$

S_1			**1000**			
S_2		**1001**	**1010**	**1100**	**0000**	
S_3	**1011**	**1101**	**0001**	**1110**	**0010**	**0100**
S_4		**0110**	**0101**	**0011**	**1111**	
S_5			**0111**			

FIG. 10. For a pattern with $d_M = 4$ we arrange the four determinant bits as they contribute to the five groups $S_1, \ldots, S_5$ for the case that the determinant bits of S_1 are **1000**, corresponding to Fig. 9.

where we have supposed that the fluctuations of $n(G)$ are small. If i is a nondeterminant bit position, the arguments leading to Eq. (15) do not apply, but following a different line we obtain $\overline{R}_i \approx 0$, as explained above.

For the example shown in Fig. 9 we know from simulations that a static pattern occurs where all nodes of S_2 are occupied and the others are empty, that is, $n(G) = n(S_2)$. This leads to $\overline{R}_i \approx 0.5\, r_i(v_1)$.

For the typical case of a symmetry-breaking pattern, the R_i make it possible to identify the determinant bits directly and in real time. This procedure is remarkably robust against defects in the pattern. For symmetric patterns, for example, $n(S_1 \cup S_2) = n(S_4 \cup S_5)$ in the above example, Eq. (15) gives $\overline{R}_i = 0$; determinant and nondeterminant bits cannot be distinguished this way.

V. ARCHITECTURE OF SPECIFIC PATTERNS

In the previous section we derived the structural properties. Here we apply these results to a zoo of specific patterns observed in simulations on $G_{12}^{(2)}$ with $[t_L, t_U] = [1,10]$. This restriction allows a certain completeness of the overview. For other parameters different patterns can be found, but inspection of several examples indicates that the building principles generally apply.

We start with the static patterns with $d_M = 2$, 4, and 6 and point out their common properties. We show how the concept of pattern modules needs to be extended to explain a more sophisticated static pattern. Finally, we describe the complex dynamic pattern which is built of modules of dimension $d_M = 11$. For all examples below and a few more cases the link matrices are explicitly listed in [82].

A. Simple static patterns

The simplest static pattern is the $d_M = 2$ pattern with characteristic two clusters, discussed in detail in Sec. IV A. For the ideal pattern Eq. (15) gives $\overline{R}_i \approx 1\, r_i(v_1)$ for both determinant bit postions; all other $\overline{R}_i \approx 0$, which is in accordance with simulation.

In the static regime, for $0 < p \lessapprox 0.03$, we frequently observed a pattern with eight clusters. It can be described with a pattern module of dimension $d_M = 4$.

It has five groups, which are illustrated in Fig. 11 together with their links according to the link matrix [Eqs. (8) and (9)]. Group S_2 is highly occupied and its nodes form the eight clusters (Fig. 12). S_3, S_4, and S_5 are the groups of stable holes and S_1 is the group of singletons. Note the symmetry of the structure in the figure, by which we could swap the groups S_2 and S_4, and the groups S_1 and S_5. The same symmetry is reflected in the binomial coefficients in the formula for the group sizes [Eq. (7)] and can be seen in the link matrix [cf. Eq. (11)].

The number of occupied nodes according to Eq. (7) is $|S_2| = \binom{4}{2-1} \times 2^8 = 1024$ and the number of singletons (unstable holes) is $|S_1| = \binom{4}{1-1} \times 2^8 = 256$. The group of stable holes consists of three subgroups, the total number of stable holes is given by $|S_3| + |S_4| + |S_5| = (6 + 4 + 1) \times 2^8 = 2816$. This is in agreement with the observations given in Table I.

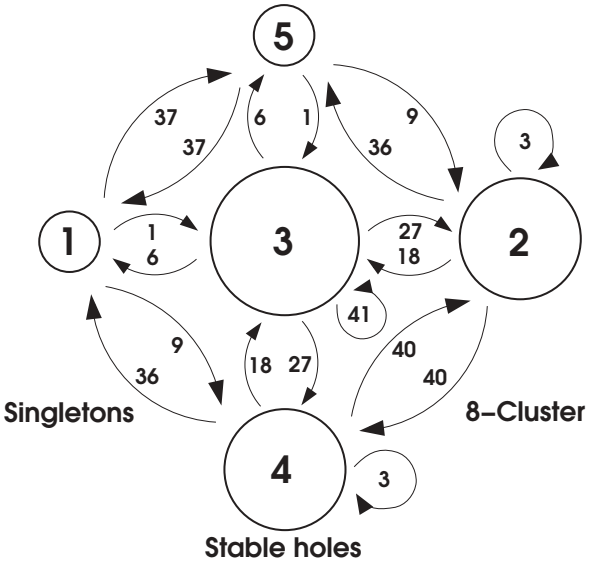

FIG. 11. Detailed view of the architecture of the eight-cluster pattern. As in Fig. 5 the circle sizes correspond to the group sizes. The arrows and the numbers next to them indicate how many nodes of a group exert influence on the nodes of another group according to the link matrix.

For $0 < p \lessapprox 0.03$ we find occasionally a $d_M = 6$ pattern with characteristic 30 clusters. It is rare, but once established it remains stable for a long time. For the determinant bit positions in the ideal pattern Eq. (15) yields $\overline{R}_i \approx 0.33\, r_i(v_1)$ as in simulations.

Its seven groups and their linking are schematically shown in Fig. 13. Each node in group S_3 has six links within the group. Thus, a completely occupied S_3 is stable. There are $\binom{6}{2} = 15$ nodes in the pattern module which belong to S_3. These are linked to the corresponding 15 nodes of the opposite module, thus forming the 30 cluster. The stable hole groups S_4 to S_7 are suppressed; S_1 and S_2 are singletons.

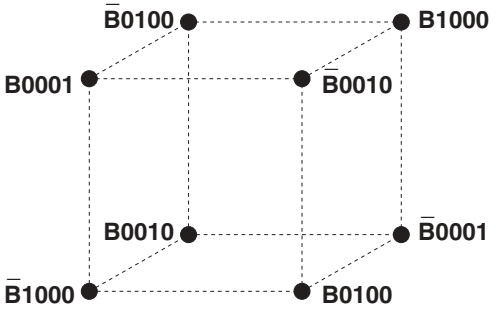

FIG. 12. A cluster of eight occupied nodes as found in a snapshot of the occupied subgraph in the $d_M = 4$ architecture. It has the topology of a cube in three dimensions. The cluster consists of nodes in S_2, which are all occupied up to few defects. The nodes are labeled with their bit strings. The four digits represent the determinant bits. For simplicity and readability we give the determinant bits of the architecture realization in which S_1 has determinant bits **0000**. **B** represents the string of nondeterminant bits, and $\overline{\mathbf{B}}$ represents its inverse. All links have two mismatches.

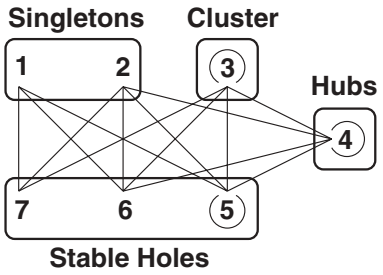

FIG. 13. The architecture of the 30-cluster pattern. As in Fig. 8 the lines show possible links between nodes of the groups.

These simple static patterns $d_M = 2, 4, 6$ have in common a very regular structure and a mechanism of self-support and suppression. There is one fully occupied core group with a self-coupling within the threshold window $[t_L,t_U] = [1,10]$. Its nodes form clusters, sustain themselves, and suppress all other groups except for the singletons, which are surrounded by stable holes only. The occupation of singletons increases slowly with increasing influx p. Since singletons have only weakly occupied neighbors (stable holes) they are a hypothetical place for self. However, these patterns have only a very limited adaptivity.

At $p = 0$ the group of singletons will be emptied, the remaining occupied nodes which are connected to at least t_L occupied nodes survive. An influx $p \gtrsim 0$ perturbs the pattern and tests its stability. Increasing p further leads to more and more defects until, finally, the whole pattern will be destabilized.

All patterns observed in simulations can be well explained with the concept of pattern modules. On the contrary, not all patterns that can be constructed with pattern modules, have been actually observed. For many unobserved patterns we can explain why they are either forbidden or very rare.

By the pattern module $d_M = 8$ we can construct a static 112-cluster pattern in the same manner as 2-, 8-, and 30-cluster patterns. We occupy the core group S_4, which consists of clusters of size 112. Each node in such a cluster has 10 occupied neighbors, all within S_4. A small perturbation by occupying an additional neighbor destabilizes the pattern. This is the reason for its rareness. For even $d_M \geqslant 10$ the number of links within the core group exceeds t_U so that a completely occupied core is impossible.

For odd d_M the self-coupling of the core groups is so strong, $L_{ii} \geqslant 12 > t_U$ (cf. [82]), that static patterns with one completely occupied group are excluded. We could increase t_U to allow some of these static patterns.

For our choice of $m = 2$ in patterns with $d_M \geqslant 7$ there are groups, at the end of the tail of the caterpillar, outside the range of influence of the core. An occupied core is not able to suppress these groups. The range of influence could be increased by increasing m.

B. Static pattern with two modules

There are static patterns that cannot be explained with a single module, but by an extension of the concept to two pattern modules. We explain this with the following example.

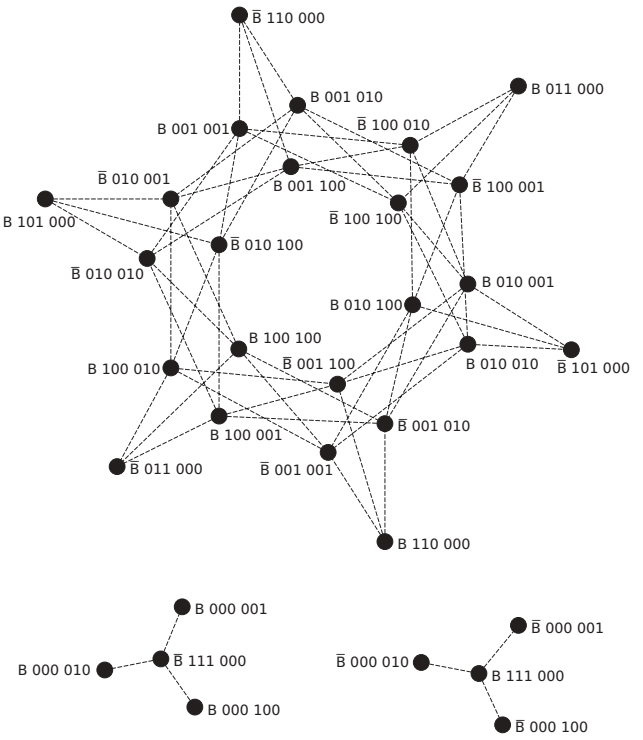

FIG. 14. A 24 cluster and two 4 clusters as observed in a snapshot of the occupied subgraph in the 2 module architecture with $d_M = d'_M = 3$. The nodes are labeled with their bit strings. The nondeterminant bits are subsumed under **B** or its inverse $\overline{\mathbf{B}}$, respectively. The two groups of three digits represent the determinant bits, corresponding to the first and second modules. For readability the determinant bits are chosen such that group $S_1 \otimes S'_1$ is encoded by **000 000**. All links have two mismatches. Figure created using yEd [80].

In the regime of static patterns $0 < p \lessapprox 0.035$, we often find a pattern that is characterized by large star-shaped clusters of size 24 and accompanying small clusters of size 4 with one central node surrounded by three separate nodes attached to it (cf. Fig. 14).

It has six determinant bits, but the structure cannot be explained by a single pattern module of dimension 6. However, an architecture constructed with two pattern modules of dimension d_M and d'_M with $d_M = d'_M = 3$ is in full agreement with the observation.

A node group is now denoted by $S_i \otimes S'_j$; the former corresponds to the first module, the latter to the second one. The group $S_1 \otimes S'_1$ has determinant bits $\boldsymbol{b}_1\boldsymbol{b}_2\boldsymbol{b}_3$ $\boldsymbol{b}'_1\boldsymbol{b}'_2\boldsymbol{b}'_3$; in the example given in Fig. 14 we have chosen **000 000**. The index k of S_k has the same meaning as for a single module. The determinant bits of group $S_i \otimes S'_j$ deviate in $i-1$ bits from $\boldsymbol{b}_1\boldsymbol{b}_2\boldsymbol{b}_3$ and in $j-1$ bits from $\boldsymbol{b}'_1\boldsymbol{b}'_2\boldsymbol{b}'_3$. The deviations in the first set of bits are independent from those in the second set of bits. Therefore, not only seven groups are generated as for a single module of $d_M = 6$, but we find $(d_M + 1)(d'_M + 1) = 4 \times 4 = 16$ groups. The relative size of group $S_i \otimes S'_j$ is $\binom{d_M}{i-1}\binom{d'_M}{j-1}$. Also the link matrix can be calculated. The number of links from a node $v_{ij} \in S_i \otimes S'_j$

to nodes in $S_r \otimes S'_s$ is given by

$$L_{ij,rs} = \sum_{l,k,k'=0} \Bigg[\binom{d - d_M - d'_M}{l} \times \binom{i-1}{k + \max(0, -\Delta_{ij})} \binom{d_M - i + 1}{k + \max(0, \Delta_{ij})} \times \binom{r-1}{k' + \max(0, -\Delta'_{rs})} \binom{d'_M - r + 1}{k' + \max(0, \Delta'_{rs})} \times \mathbb{1}(l + 2k + 2k' + |\Delta_{ij}| + |\Delta'_{rs}| \leqslant m) \Bigg], \quad (16)$$

where $\Delta'_{rs} = d'_M - r - s + 2$ in analogy to Δ_{ij}. This is a condensed notation for the four cases discriminated by $\Delta_{ij}, \Delta'_{rs} \gtrless 0$.

We obtain the ideal 24 clusters if we occupy the groups $S_2 \otimes S'_2$ for the nodes on the ring and $S_3 \otimes S'_1$ for the peripheral nodes. Similarly, the small 4 clusters are build of occupied groups $S_4 \otimes S'_1$ as the central node and $S_1 \otimes S'_2$ as the attached nodes. In this static pattern more than one group is occupied. These groups mutually stimulate each other instead of supporting themselves.

For two modules the center of mass components R_i differ not only between determinant and nondeterminant bit positions, but also between determinant bits belonging to different modules. For the determinant bit at position i Eq. (15) becomes

$$\overline{R}_i \approx \left[\frac{1}{\overline{n}(G)} \sum_{j=1}^{d_M+1} \sum_{j'=1}^{d'_M+1} \frac{d_M^{(\prime)} - 2j^{(\prime)} + 2}{d_M^{(\prime)}} \overline{n}(S_j \otimes S'_{j'}) \right] r_i(v_{1,1}), \quad (17)$$

where $r_i(v_{1,1})$ is the position vector component of a node in $S_1 \otimes S'_1$ and the prime in parentheses at $d_M^{(\prime)}$ and $j^{(\prime)}$ applies only if i is a position in the second module. For our pattern with $d_M = d'_M = 3$ we obtain $\overline{R}_i \approx 0.25$ for the first module and $\overline{R}_i \approx 0.50$ for the second.

An extension to several modules of possibly different dimension appears natural.

C. Dynamic pattern

In simulations starting from the empty base graph for $p \gtrapprox 0.03$ we only find a dynamical, stationary pattern with complex architecture. It was first observed in simulations in [13]. There, six groups of nodes sharing statistical properties were identified and the architecture was described on a phenomenological base. There are groups of singletons, stable holes, two peripheral groups, and two core groups. A snapshot of the occupied nodes and their linking is given in Fig. 3.

All structural properties, namely the number and size of the groups and their linking, can be explained within the concept of pattern modules using pattern modules of $d_M = 11$. This leads to 12 groups, which for a certain range of p can be merged to the 6 phenomenological groups above. Groups S_1 to S_3 are groups of singletons, and groups S_8 to S_{12} are stable holes [see Fig. 15 (top) and Table III].

Table III in the first two rows gives the mapping from the 12 groups S_i to the 6 groups $\widetilde{S}_j$ found empirically in [13]. The derived group sizes $|S_i|$ are in excellent agreement with the measured group sizes. Also, the sizes of the subgroups S_8, S_9, S_{10}, S_{11}, and S_{12} correctly sum up to 1124, which is exactly the statistically measured number of stable holes (see Table I in [13]). Besides the structural information, Table III also shows group averages of local node characteristics, such as mean lifetime and mean occupation. For the group occupations $\langle \overline{n}(v) \rangle_{S_i}$ for $p = 0.028$ given in Table III we can determine R_i, for the determinant bits Eq. (15) and direct observation give $\overline{R}_i \approx 0.29$.

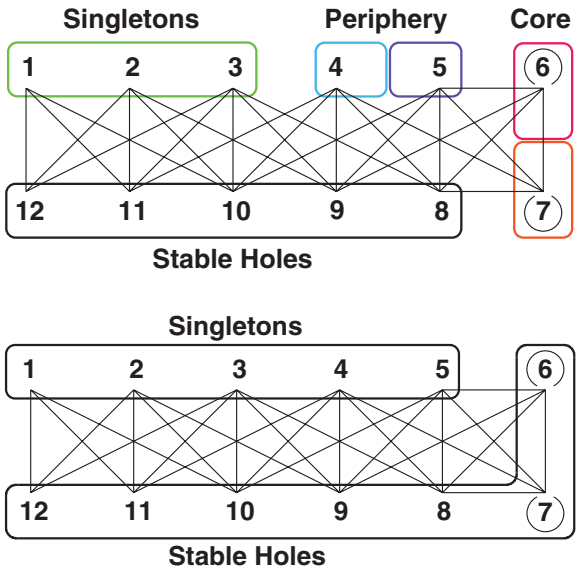

FIG. 15. (Color online) Visualization of the 12-group structure for $0.03 \lessapprox p \lessapprox 0.045$ (top) and for $p \gtrapprox 0.045$ (bottom). As in Fig. 8 the lines show possible links between nodes of the groups. The coloring of the groups in the upper figure corresponds to the color of the respective nodes in Fig. 3, according to the qualitative classification.

We calculated the link matrix for this pattern (cf. Table IV). In contrast to the static patterns that emerge for low influx p in this structure we also find perfect matches and one-mismatch links, but they are simply outnumbered by the two-mismatch links.

The structural properties and the mean occupation of the groups obtained in simulations make it possible to understand the qualitative behavior. The phenomenological classification in holes, singletons, etc., depends on p.

For a range $0.03 \lessapprox p \lessapprox 0.045$ the following qualitative groups appear. There are *stable holes* as in static patterns. *Singletons* are surrounded by stable holes. *Core groups* couple to all groups except for singletons. The number of self-couplings is larger than the upper threshold t_U. Therefore, a complete occupation is not stable. However, there are many configurations of partial occupation. The *periphery* couples to the core groups and to stable holes. It is stimulated by stable holes, which are momentarily occupied during the influx step, and by the stationary occupied core. It is the group with the highest occupation. The core groups have more links to occupied groups than the periphery and therefore its mean occupation is smaller than that of the periphery.

Although the pattern only evolves for $p \gtrapprox 0.03$, the connected part of the network, the giant cluster, survives if the

TABLE III. The node characteristics of the 12-groups structure. Data from 500,000 iterations for $p = 0.028$.

Qualitative classification	Singletons			Periphery		Core		Stable holes				
Group	S_1	S_2	S_3	S_4	S_5	S_6	S_7	S_8	S_9	S_{10}	S_{11}	S_{12}
Phenomenological group [13]	$\widetilde{S}_4$	$\widetilde{S}_4$	$\widetilde{S}_4$	$\widetilde{S}_5$	$\widetilde{S}_6$	$\widetilde{S}_3$	$\widetilde{S}_2$	$\widetilde{S}_1$	$\widetilde{S}_1$	$\widetilde{S}_1$	$\widetilde{S}_1$	$\widetilde{S}_1$
Group size $\lvert S_i \rvert$	2	22	110	330	660	924	924	660	330	110	22	2
Mean occupation $\langle \overline{n}(v) \rangle_{S_i}$	0.206	0.193	0.193	0.321	0.477	0.069	0.030	0.000	0.000	0.000	0.000	0.002
Mean lifetime $\langle \overline{\tau}(v) \rangle_{S_i}$	9.11	8.53	8.56	16.86	32.55	2.66	1.10	0.00	0.00	0.00	0.00	0.07
Occupied neighbors $\langle \overline{n}(\partial v) \rangle_{S_i}$	0.01	0.01	0.01	0.84	1.88	8.94	10.56	19.63	19.66	27.78	21.05	15.27

influx is stopped. Since $t_L = 1$, all isolated nodes disappear. Starting with a small $p \lessapprox 0.03$ from the giant cluster leads to a similar scenario as described in Sec. III A, where the giant cluster decays. This shows that the dynamic pattern requires a sufficiently high influx to emerge and to remain stationary. The influx permanently tests the stability of this pattern against random perturbations.

Increasing the influx above $p \gtrapprox 0.045$ also the core groups are suppressed by a growing population of peripheral nodes. The occupation of the core groups thus converges to the occupation of the stable holes while in the same process the occupation of peripheral groups and singletons converges. Thus, based on the same pattern module as above we can distinguish considering mean occupation and lifetime only two groups, stable holes and singletons [cf. Fig. 15 (bottom)]. Note, that taking the number of occupied neighbors into account we can still distinguish groups $S_6, \ldots, S_9$.

For even higher $p \gtrapprox 0.07$ the dynamic pattern becomes transient. It often breaks down and rebuilds with a different orientation on the base graph. Nodes can no longer be permanently assigned to one of the 12 groups, but they change their group membership with every new formation of the pattern. Thus, a statistical characterization of nodes by temporal averages is impossible.

For still larger $p \gtrapprox t_U/\kappa = 0.127$ the dynamics is completely dominated by the random influx. The graph is so densely occupied after the influx that typically the upper threshold of the window rule is exceeded.

For $d_M \geqslant 7$ holes at the tail of the caterpillar are not sufficiently suppressed by the core, cf. the discussion at the end of Sec. V A and Fig. 8. Suppression by the periphery, $d_M \geqslant 7$, and by singletons, $d_M \geqslant 11$, is required. Otherwise, these holes could become occupied, which would destabilize the complete pattern. Since singletons need sufficient influx, those patterns occur only for higher p. Interestingly, among several candidates only the dynamic pattern with $d_M = 11$ has been observed on $G_{12}^{(2)}$ for our setting of $[t_L, t_U]$ and $0 < p < 0.11$. It is also the only observed pattern with odd module dimension.

In this context we recall that the autonomous dynamics of the idiotypic network was a truly central feature of Jerne's original concept [4]. The existence of core and periphery fits perfectly to the second generation idiotypic networks of Varela and Coutinho [6].

TABLE IV. Link matrix for $d_M = 11$. Missing entries are zero. This is an instance for the general structure shown in Fig. 7.

	S_1	S_2	S_3	S_4	S_5	S_6	S_7	S_8	S_9	S_{10}	S_{11}	S_{12}
v_1										55	22	2
v_2									45	20	12	2
v_3								36	18	20	4	1
v_4							28	16	26	6	3	
v_5						21	14	30	8	6		
v_6					15	12	32	10	10			
v_7				10	10	32	12	15				
v_8			6	8	30	14	21					
v_9		3	6	26	16	28						
v_{10}	1	4	20	18	36							
v_{11}	2	12	20	45								
v_{12}	2	22	55									

VI. CONCLUSIONS

We considered a minimalistic model [13] of the idiotypic network which evolves towards a complex functional architecture. The main mechanisms are the random influx of new idiotypes and the selection of not sufficiently stimulated idiotypes. Numerical simulations have shown that after a transient period a steady state with a specific architecture is reached. Generally, groups of nodes sharing statistical properties can be identified, which are linked in a characteristic way.

In the present paper we achieved a detailed analytical understanding of the building principles of the emerging patterns. Modules of remarkable regularity serve as building blocks. We can calculate size and connectivity of the groups in agreement with numerical simulations.

The described building principles are formulated generalizing regularities found by a careful analysis of the simplest pattern. The architectures of all patterns observed so far can be described by these simple building principles.

With increasing influx p we observe a transition from a static regime (periodic patterns with defects) to a dynamic regime (stationary architecture with groups of nodes sharing statistical properties with fluctuating occupation). With further increasing influx, in the random regime, the nodes no longer remain in definite groups for a longer period of time (cf. Fig. 4).

With all necessary caution we could ask, "What is the working regime of the model network?"

The perfect $d_M = 2$-pattern of idiotype–anti-idiotype pairs is stable and complete: Every node of the base graph has at least one occupied neighbor. Any antigen is surely recognized, including the self, which implies autoimmune reactions. The $d_M = 4$-pattern and the other static patterns with $d_M > 4$

contain a group of singletons surrounded by stable holes, which provides room for self [83]. However, these patterns are essentially static with few dynamic defects. They are very rigid and therefore not adaptive.

This is in contrast to the dynamic regime, where we have a stationary architecture with a densely connected core, a periphery, and singletons. The nodes stay within the corresponding groups but their occupation is dynamic [84], which allows adaptation and plasticity. The influx is necessary for the emergence of the dynamic pattern; it permanently tests its stability and sustains the pattern.

A network that consists of a central and a peripheral part is envisaged in the concept of second generation idiotypic networks [6]. The central part is thought to play an essential role, for example, in the control of autoreactive clones; the peripheral part is thought to provide the response to external antigens and to keep a localized memory. An *ad hoc* architecture similar to the one described here was used in [85] to investigate the role of the idiotypic network in autoimmunity.

As discussed above, the influx of new idiotypes decides which pattern emerges. If we stop the influx, once a pattern has established, occupied singletons disappear as well as isolated occupied nodes from other groups. All other components of the network freeze, for example, in the $d_M = 11$-architecture the connected occupied nodes of core and periphery. Now a sufficiently small influx would test the stability of this pattern but is not enough to sustain it; the pattern decays and a static pattern corresponding to the new influx emerges. Starting from a static pattern, increasing the influx raises the number of defects. For an influx high enough the static pattern disappears and a dynamic one emerges.

While the model is clearly immunologically inspired, it is worth pointing out that the results are interesting in themselves. The process of self-ordering is genuinely evolutionary. The local processes of addition and deletion of nodes involve randomness (random influx) and selection (window rule), they have a global impact. On a longer time scale we observe an evolution towards a complex architecture. Depending on the parameters this architecture can consist of many regularly arranged small modules or of few large modules covering the complete base graph. Most interestingly, for a range of parameters, we find a dynamic stationary pattern comprising a central and a peripheral part. Also, evolved real world networks like internet [86] and brain [87] exhibit central and peripheral parts. The analytical understanding of the principles opens the possibility to consider networks of biological size and to investigate their scaling behavior, for example, exploiting renormalization group techniques (cf. [88]).

We emphasize that the model investigated in this paper is minimalistic and of high symmetry. Some extensions of the model appear natural, for example, weighting the links depending on the number of mismatches, using bit strings of different lengths, allowing parallel translations of bit strings, or deleting links randomly. This reduces the symmetry of the base graph and may change the density of the linking. The base graph is then not necessarily regular; that is, nodes can have a different number of links. Further, several levels of occupation could be allowed. Some of these extensions seem necessary to investigate certain immunologically motivated problems. First results of simulations on models modestly modified along these lines show that groups of nodes sharing statistical properties organized in a stationary architecture exist and indicate that the concept of pattern modules still applies [89,90].

Ongoing studies investigate the evolution of the network in the presence of a permanent self-antigen or an invading foreign antigen. In the dynamic regime the network organizes such that the self has only rarely occupied neighbors [89]. In the static regime bistable stationary states are found such that a foreign antigen induces a transition from one state to another (memory) state [89,90]. More details will be reported elsewhere.

We also want to study the changes in the architecture during the lifetime of an individual. Further variations of the dynamics include hypermutation during cell proliferation [91] and a delay of deletion of unstimulated clones.

In a forthcoming article [92] we report on a modular mean field theory to compute statistical group characteristics for arbitrary parameters and any given pattern. The mean occupation, the mean lifetime, and the mean occupation of the neighborhood are in good agreement with the simulations.

ACKNOWLEDGMENTS

Thanks are due to Andreas Kühn, Heinz Sachsenweger, Benjamin Werner, and Sven Willner for valuable comments. H.S. thanks the IMPRS Mathematics in the Sciences and the Evangelisches Studienwerk Villigst e.V. for funding.

APPENDIX: SCALING OF THE RELATIVE GROUP SIZE WITH INCREASING SYSTEM SIZE

Suppose the biological system can express about 10^{11} different genotypes for antibodies [3]. This would correspond to a bit string length $d = 36$. The system size in simulations is limited by the computer resources. Still, today the biological system size is hard to reach. On the other hand, the thermodynamic limit is not of interest, because the biological system is large but finite. Therefore, the scaling of qualitative properties with increasing system size is important.

In the following we consider patterns with odd $d_M = d - 1$. For $d_M \geqslant 7$ we find from the "caterpillar representation" (cf. Fig. 8) an architecture of two core groups, two peripheral groups, and several groups of stable holes and of singletons. With increasing d only the tail of the caterpillar grows, that is, the number of stable hole and singleton groups increases. How does the relative size of the different qualitative groups scale with d?

The size of the groups is given by Eq. (7), which reduces for $d_M = d - 1$ to

$$|S_i| = 2\binom{d-1}{i-1}, \quad i = 1, \ldots, d. \tag{A1}$$

We can order the groups with increasing i; then the two core groups are the two central groups for $i = d/2 - 1$ and $d/2$, which both have the same size. Thus, the total size of the

core groups is

$$|C| = 2^2 \binom{d-1}{d/2}. \tag{A2}$$

The peripheral groups are the two groups to the left of the core groups, $i = d/2 - 2$ and $d/2 - 3$, which have the total size

$$|P| = 2\left[\binom{d-1}{d/2-2} + \binom{d-1}{d/2-3}\right]. \tag{A3}$$

Elementary algebra yields

$$|P| = \frac{d(d-2)}{(d+2)(d+4)}|C|. \tag{A4}$$

To the left of the peripheral groups are the groups of singletons, S, and to the right of the core groups are all groups of stable holes, H (cf. Table III for the example with $d = 12$).

Because of $\binom{n}{m} = \binom{n}{n-m}$ we have

$$|H| = |S| + |P| \tag{A5}$$

and obviously

$$|S| + |P| + |C| + |H| = |G_d| = 2^d. \tag{A6}$$

With this knowledge we infer

$$|H| = 1/2(|G_d| - |C|) \tag{A7}$$

and

$$|S| = |H| - |P|. \tag{A8}$$

For large d we obtain in Stirling approximation

$$|C| \approx \sqrt{\frac{2}{\pi}} 2^{d+1} \frac{1}{\sqrt{d}}\left(1 - \frac{3}{4d^2} + \cdots\right). \tag{A9}$$

Thus, the relative size scales with d as

$$|\widetilde{C}| = \frac{|C|}{|G_d|} \approx 2\sqrt{\frac{2}{\pi}} \frac{1}{\sqrt{d}}\left(1 - \frac{3}{4d^2}\right) \sim d^{-1/2}. \tag{A10}$$

In the thermodynamic limit $|\widetilde{C}|$ and $|\widetilde{P}|$ tend to zero. For a realistic size of the network, for example, $d = 36$, we have for the qualitative groups $|\widetilde{C}| \approx 0.266$, $|\widetilde{P}| \approx 0.214$, $|\widetilde{H}| \approx 0.367$, and $|\widetilde{S}| \approx 0.153$. $|\widetilde{C}|$ and $|\widetilde{P}|$ together account for a half of all nodes. Of course, the parameters p and $[t_L, t_U]$ have to be suitably adjusted such that a pattern of the supposed architecture actually emerges.

[1] F. Burnet, *The Clonal Selection Theory of Acquired Immunity* (Vanderbuilt University Press, Nashville, TN, 1959).

[2] S. Tonegawa, Nature (London) **302**, 575 (1983).

[3] C. Berek and C. Milstein, Immunol. Rev. **105**, 5 (1988).

[4] N. Jerne, Ann. Inst. Pasteur Immunol. C **125**, 373 (1974). Immunol. Rev. **79**, 5 (1984).

[5] A. Coutinho, Immunol. Rev. **110**, 63 (1989).

[6] F. Varela and A. Coutinho, Immunol. Today **5**, 159 (1991).

[7] A. Coutinho, Biol. Res. **36**, 17 (2003).

[8] J. Carneiro, Ph.D. thesis, University of Porto, 1997.

[9] U. Behn, Immunol. Rev. **216**, 142 (2007).

[10] U. Behn, in *Encyclopedia of Life Sciences* (John Wiley & Sons, Chichester, 2011).

[11] J. M. Reichert, Monoclonal Antibodies **3**, 76 (2011).

[12] A. Madi, D. Y. Kenett, S. Bransburg-Zabary, Y. Merbl, F. J. Quintana, A. I. Tauber, I. R. Cohen, and E. Ben-Jacob, PLoS ONE **6**, e17445 (2011).

[13] M. Brede and U. Behn, Phys. Rev. E **67**, 031920 (2003).

[14] Representation of idiotypes by bitstrings was proposed by J. Farmer, N. Packard, and A. Perelson, Physica D **22**, 187 (1986); See also, however, N. Jerne, EMBO J. **4**, 847 (1985).

[15] Complementarity of the binding sites of real antibodies means matching of the ternary structures of the proteins, where the spatial structure and van der Waals, electrostatic, hydrophobic, and hydrophilic interactions are involved. To describe this is beyond the scope of this paper.

[16] In the original version [13] a constant number I of new idiotypes was added in each influx step. Here we prefer to occupy empty nodes with a given probability p. This roughly corresponds to the transition from a microcanonical to a canonical approach in statistical physics.

[17] A. Perelson and G. Weisbuch, Rev. Mod. Phys. **69**, 1219 (1997).

[18] The random filling of a fraction of the base graph—without the window rule—leads to the percolation problem treated in [88]. Asking for the number of configurations of occupied nodes which survive the window rule is a question interesting in itself. Disconnected clusters survive independently; hence, the number of surviving configurations (preserving immunological memory) is combinatorially large. Imposing constraints, like optimal covering of the base graph, will reduce this number but complicates the problem considerably. The iteration, which enables evolution, completes the model.

[19] Preliminary accounts were given in H. Schmidtchen and U. Behn, in *Artificial Immune Systems ICARIS 2006*, Lecture Notes in Computational Sciences Vol. 4163, edited by H. Bersini and J. Carneiro (Springer-Verlag, Berlin Heidelberg, 2006), pp.–81–94; in *Mathematical Modeling of Biological Systems*, edited by A. Deutsch, R. Bravo de la Parra, R. de Boer, O. Diekmann, P. Jagers, E. Kisdi, M. Kretzschmar, P. Lansky, and H. Metz (Birkhäuser, Boston, 2008), Vol. II, pp. 157–167.

[20] S. Strogatz, Nature (London) **410**, 268 (2001).

[21] S. Dorogovtsev and J. Mendes, *Evolution of Networks: From Biological Nets to the Internet and WWW* (Oxford University Press, Oxford, 2003).

[22] A.-L. Barabási and R. Albert, Rev. Mod. Phys. **74**, 47 (2002).

[23] R. Albert, H. Jeong, and A.-L. Barabási, Nature (London) **406**, 378 (2000).

[24] E. de Silva and M. P. H. Stumpf, J. R. Soc. Interface **2**, 419 (2005).

[25] S. Boccaletti, V. Latora, Y. Moreno, M. Chavez, and D.-U. Hwang, Phys. Rep. **424**, 175 (2006).

[26] M. E. J. Newman, *Networks: An Introduction* (Oxford University Press, Oxford, 2010).

[27] G. Caldarelli, *Scale-Free Networks* (Oxford University Press, Oxford, 2007).

[28] K. Deng and Y. Tang, Chin. Phys. Lett. **21**, 1858 (2004).

[29] M. Salathé, R. M. May, and S. Bonhoeffer, J. R. Soc. Interface **2**, 533 (2005).

[30] J. L. Slater, B. D. Hughes, and K. A. Landman, Phys. Rev. E **73**, 066111 (2006).

[31] C. Moore, G. Ghoshal, and M. E. J. Newman, Phys. Rev. E **74**, 036121 (2006).

[32] E. Ben-Naim and P. L. Krapivsky, J. Phys. A **40**, 8607 (2007).

[33] Y. Gu and J. Sun, Phys. Lett. A **372**, 4564 (2008).

[34] B. Kim, A. Trusina, P. Minnhagen, and K. Sneppen, Eur. Phys. J. B **43**, 369 (2005).

[35] M. J. Alava and S. N. Dorogovtsev, Phys. Rev. E **71**, 036107 (2005).

[36] H. Seyed-allaei, G. Bianconi, and M. Marsili, Phys. Rev. E **73**, 046113 (2006).

[37] S. N. Dorogovtsev and J. F. F. Mendes, Europhys. Lett. **52**, 33 (2000).

[38] J. Wang and P. De Wilde, Phys. Rev. E **70**, 066121 (2004).

[39] C. Zhu, A. Kuh, J. Wang, and P. De Wilde, Phys. Rev. E **74**, 046109 (2006).

[40] K. Park, Y.-C. Lai, and N. Ye, Phys. Rev. E **72**, 026131 (2005).

[41] S. Laird and H. J. Jensen, Europhys. Lett. **76**, 710 (2006).

[42] T. Hruz, M. Natora, and M. Agrawal, Phys. Rev. E **77**, 046101 (2008).

[43] S. N. Dorogovtsev and J. F. F. Mendes, Phys. Rev. E **63**, 056125 (2001).

[44] R. V. Solé, R. Pastor-Satorras, E. Smith, and T. B. Kepler, Adv. Complex Syst. **5**, 43 (2002).

[45] J. Davidsen, H. Ebel, and S. Bornholdt, Phys. Rev. Lett. **88**, 128701 (2002).

[46] K. Klemm and V. M. Eguíluz, Phys. Rev. E **65**, 057102 (2002).

[47] N. Sarshar and V. Roychowdhury, Phys. Rev. E **69**, 026101 (2004).

[48] C. Cooper, A. Frieze, and J. Vera, Internet Math. **1**, 463 (2004).

[49] D. Shi, L. Liu, S. X. Zhu, and H. Zhou, Europhys. Lett. **76**, 731 (2006).

[50] T. Gross and B. Blasius, J. R. Soc. Interface **5**, 259 (2008).

[51] T. Gross and H. Sayama (editors), *Adaptive Networks: Theory, Models, and Data* (Springer, Heidelberg, 2009).

[52] S. A. Kauffman, *The Origins of Order* (Oxford University Press, Oxford, 1993).

[53] A. Ilachinsky, *Cellular Automata: A Discrete Universe* (World Scientific, Singapore, 2001).

[54] M. Gardner, Sci. Am. **223**, 120 (1970).

[55] C. Bays, Complex Syst. **1**, 373 (1987); **16**, 381 (2006).

[56] C. Bays, in [64], Chap. 17, pp. 319–330.

[57] C. Bays, Complex Syst. **8**, 127 (1994); **15**, 245 (2005).

[58] N. Owens and S. Stepney, in *Game of Life Cellular Automata*, edited by A. Adamatzky (Springer-Verlag, London, 2010), pp. 331–378.

[59] S.-Y. Huang, X.-W. Zou, Z.-J. Tan, and Z.-Z. Jin, Phys. Rev. E **67**, 026107 (2003).

[60] D. Griffeath, in *Probability and Phase Transitions*, edited by G. Grimmet (Kluwer Academic Publishers, 1994) pp. 49–67.

[61] K. M. Evans, Ph.D. thesis, University of Wisconsin Madison, 1996.

[62] K. M. Evans, in *Discrete Models: Combinatorics, Computation, and Geometry, DM-CCG 2001*, DMTCS Proceedings, Vol. AA, edited by R. Cori, J. Mazoyer, M. Morvan, and R. Mosseri (Maison de l'Informatique et des Mathématiques Discrètes, Paris, France, 2001), pp. 177–192.

[63] L. S. Schulman and P. E. Seiden, J. Stat. Phys. **19**, 293 (1978).

[64] A. Adamatzky, (editor), *Game of Life Cellular Automata* (Springer-Verlag, London, 2010).

[65] J. Stewart and F. Varela, J. Theor. Biol. **153**, 477 (1991).

[66] V. Detours, H. Bersini, J. Stewart, and F. Varela, J. Theor. Biol. **170**, 401 (1994).

[67] In [65] regular arrays of idiotype–anti-idiotype populations are observed, reminiscent in a sense of our two-cluster pattern.

[68] H. Bersini, in *Advances in Artificial Life*, Lecture Notes in Computer Science Vol. 2801, edited by W. Banzhaf, J. Ziegler, T. Christaller, P. Dittrich, and J. Kim (Springer, Berlin/Heidelberg, 2003), pp. 164–174.

[69] E. Hart, in *Artificial Immune Systems ICARIS 2006*, Lecture Notes in Computational Sciences Vol. 4163, edited by H. Bersini and J. Carneiro (Springer-Verlag, Berlin, Heidelberg, 2006), pp. 66–80.

[70] G. Parisi, Proc. Natl. Acad. Sci. USA **87**, 429 (1990).

[71] A. Barra and E. Agliari, J. Stat. Mech.: Theory Exp. (2010) P07004.

[72] A. Barra and E. Agliari, Physica A **389**, 5903 (2010).

[73] A. Barra, S. Franz, and T. Sabetta, arXiv:1012.2025.

[74] L. C. Ribeiro, R. Dickman, A. T. Bernardes, and N. M. Vaz, Phys. Rev. E **75**, 031911 (2007).

[75] F. Celada and P. E. Seiden, Immunol. Today **13**, 56 (1992).

[76] R. Puzone, B. Kohler, P. Seiden, and F. Celada, Future Gener. Comput. Syst. **18**, 961 (2002).

[77] S. Forrest and C. Beauchemin, Immunol. Rev. **216**, 176 (2007).

[78] E. Hart, C. McEwan, J. Timmis, and A. Hone (editors), *Artificial Immune Systems*, Lecture Notes in Computer Science (Springer, Berlin, 2010).

[79] In this property the original version of the model [13] with a constant number of new idiotypes in each influx step can be different, obviously.

[80] yEd graph editor, v3.7, http://www.yWorks.com.

[81] For example, let $d = d_M + 1$ and $m = 2$. $\Delta_{ij} = \text{const} = 0, \pm 1, \pm 2$ for the different secondary diagonals (cf. Fig. 7). For the middle secondary diagonal we have $\Delta_{ij} = 0$, that is, $j = d_M - i + 2$. Then, $L_{i,d_M-i+2} = 2 + (i-1)(d_M + 1 - i)$, where $i = 1, \ldots, d_M + 1$. The first secondary off-diagonals are specified by $\Delta_{ij} = 1$ or -1. Their entries are given by $L_{i,d_M-i+1} = L_{d_M-i+2,i+1} = 2(d_M + 1 - i)$, where $i = 1, \ldots, d_M$. Similarly, the second secondary off-diagonals are specified by $\Delta_{ij} = 2$ or -2. Their entries are $L_{i,d_M-i} = L_{d_M-i+1,i+2} = (d_M + 1 - i)(d_M - i)/2$, where $i = 1, \ldots, d_M - 1$.

[82] See Supplemental Material at http://link.aps.org/supplemental/10.1103/PhysRevE.86.011930 for a list of link matrices.

[83] The group of singletons could be thought of as the best place for an antigen, because singletons do not have permanently occupied neighbors. However, the antigen is not completely safe there, since, before the application of the window rule, it could have an occupied neighbor (as an occupied singleton of the autonomous network has had). This could suffice to initiate an immune response. To describe this in detail the model should be refined, which is beyond the scope of this paper.

[84] Obviously, this property makes it difficult to reveal the network architecture by analyzing a single sample (a snapshot of a random selection of nodes and their mutual linking).
[85] B. Sulzer, J. van Hemmen, and U. Behn, Bull. Math. Biol. **56**, 1009 (1994).
[86] S. Carmi, S. Havlin, S. Kirkpatrick, Y. Shavitt, and E. Shir, Proc. Natl. Acad. Sci. USA **104**, 11150 (2007).
[87] S. Dehaene, J.-P. Changeux, L. Naccache, J. Sackur, and C. Sergent, Trends Cognit. Sci. **10**, 204 (2006).
[88] M. Brede and U. Behn, Phys. Rev. E **64**, 011908 (2001).
[89] B. Werner, diploma thesis, University of Leipzig, Leipzig, Germany, 2010.
[90] S. Willner, diploma thesis, University of Leipzig, Leipzig, Germany, 2011.
[91] For a NK-type model of affinity maturation, see M. W. Deem and H. Y. Lee, Phys. Rev. Lett. **91**, 068101 (2003).
[92] H. Schmidtchen and U. Behn, the following paper, Phys. Rev. E **86**, 011931 (2012).